PCCP

ROYAL SOCIETY OF CHEMISTRY

PAPER

View Article Online
View Journal | View Issue

Cite this: *Phys. Chem. Chem. Phys.*, 2025, **27**, 18870

Mind the gaps: what the STGABS27 set can teach about second-order excited state methods, solvent models, and charge transfer

Thomas Froitzheim, [a] Christof Hättig [b] and Jan-Michael Mewes *[ac]

Received 6th June 2025,
Accepted 12th August 2025

DOI: 10.1039/d5cp02144h

rsc.li/pccp

Charge-transfer (CT) states are ubiquitous in modern organic electronics, yet their accurate theoretical description poses a challenge for common excited state methods. The recently introduced STGABS27 benchmark set provides highly accurate experimentally measured adiabatic energy gaps (ΔE_{ST}) between the lowest singlet and triplet excited states of thermally activated delayed fluorescence (TADF) emitters. While first studies revealed a remarkable performance of orbital-optimized state-specific ΔDFT and mixed results with TD-DFT and DFT/MRCI, this work explores the performance of correlated wave-function methods, namely second-order algebraic diagrammatic construction (ADC(2)) and second-order approximate coupled-cluster singles and doubles (CC2) in their canonical and spin-scaled variants. Owing to the polar nature of the states, a particular emphasis is placed on the dielectric solvent models. The results show that only a few models, namely the iterative state-specific COSMO solvation model in combination with spin-component-scaled or scaled opposite-spin (SCS/SOS) ADC(2) or CC2, are competitive with ΔDFT/PCM and achieve sub-kcal mol^{-1} agreement with experimental singlet–triplet gaps, which is confirmed by cross-checks on emission energies. However, this performance comes with a hefty cost, as both models are roughly 100 times slower than similarly accurate ΔDFT/PCM-based models.

I. Introduction

Excited states that involve a substantial charge transfer (CT) are widespread throughout photochemistry, including in photoactive biological systems,[1–3] photocatalysts,[4–6] and organic electronics.[7,8] Consequently, the computational modeling of these states has gained increasing importance both in mechanistic studies and the rational design of photoactive materials.[9–15] Yet, the accurate description of CT states presents a considerable challenge for many theoretical approaches, which mainly arises from two sources: (i) the substantial change in the electronic structure upon excitation and the resulting relaxation effects, and (ii) the response of the molecular environment to the presence of typically highly polar states. Given these distinctive issues, careful benchmarking of computational protocols specifically for CT states is crucial to achieve reliable and predictive results. However, high-level theoretical reference data are scarce compared to the electronic ground state due to the minimum system size required for the spatial separation of charges.[16–21] This leaves us relying on experimental data to gain insights into CT in realistic (solvated) systems.

In this context, organic light-emitting diodes (OLEDs) that harvest triplet excitons *via* the process of thermally activated delayed fluorescence (TADF)[22–27] are a useful source of highly accurate reference values. In TADF emitters, (reverse) intersystem crossing (rISC) enables the thermal interconversion of excitons between the lowest singlet (S_1) and triplet (T_1) states and, in turn, radiative decay of triplet excitons *via* the S_1 state. The rate of this TADF process depends exponentially on both the adiabatic energy gap (ΔE_{ST}) between S_1 and T_1 and the temperature.[28] This places a severe constraint on ΔE_{ST} and, thus, the design of efficient TADF emitters. Low-lying CT states in donor–acceptor-type systems frequently exhibit the necessary small ST-gap, as the spatial separation of electron and hole minimizes the destabilizing exchange contribution for the singlet. Crucially, the magnitude of ΔE_{ST} is often accessible by temperature-dependent measurements of the TADF rate,[29] which provides high-quality reference data for theoretical benchmarking.

Exploiting this unique access to accurate experimental data for CT states, some of us presented in a recent letter the new STGABS27 benchmark set consisting of 27 emitters with measured ΔE_{ST} values.[30] Furthermore, the work showed that these

[a] *Mulliken Center for Theoretical Chemistry, University of Bonn, Beringstr. 4, 53115 Bonn, Germany*
[b] *Lehrstuhl für Theoretische Chemie, Ruhr-Universität Bochum, 44780 Bochum, Germany*
[c] *beeOLED GmbH, Gostritzer Str. 67c, 01217 Dresden, Germany. E-mail: janmewes@janmewes.de*

experimental gaps can be reproduced with remarkable accuracy of $\approx$0.5 kcal mol^{-1} (0.025 eV) by employing state-specific, orbital-optimized spin-restricted and unrestricted open-shell Kohn–Sham density functional theory (ROKS[31–36] and UKS[37,38]) in combination with a polarizable continuum model (PCM).[39,40] The best-performing combination on the STGABS27 is ROKS/PCM with the optimally tuned[41–45] range-separated hybrid OT-ωB97M-V[46,47] (used here for comparison and for brevity just denoted as ROKS/PCM) yields a mean unsigned error (MUE) of 0.022 eV and mean signed error (MSE) of $-$0.001 eV. However, since the functional dependence in ΔDFT is much less severe than for TD-DFT,[48] other functionals in combination with ROKS and even simpler spin-unrestricted approaches, *e.g.*, plain PBE0-D4[49–51] (MUE: 0.029 eV, MSE: $-$0.007 eV) or LC-ωPBE-D4[52] (MUE: 0.029 eV, MSE: $-$0.009 eV with ω = 0.175 a.u.) are nearly as accurate. In recent follow-ups, some of us showed that state-specific ROKS or UKS outclass the popular Tamm–Dancoff-approximated time-dependent density functional theory (TD(A)-DFT)[53,54] for singlet–triplet gaps[55,56] and emission energies (E_{em})[48] of the emitters in STGABS27(-EMS), and also for other sets with related multi-resonance (MR)[57] and inverted singlet–triplet gap (INVEST)[58–60] TADF emitters, where doubly excited determinants are thought to play an important role.[61,62] One particularly notable combination that crystallized in these studies is LC-ωPBE-D4/UKS with ω = 0.175–0.200 a.u. (also considered here and denoted as UKS/PCM) which, in contrast to ROKS/PCM, also performs well for singlet–triplet gaps and emission energies of MR-TADF and INVEST emitters.[61,62] Generally, the good performance and reduced functional dependence has been traced back to a particularly accurate account of orbital relaxation in the state-specific self-consistent field (SCF) procedure in ΔDFT, whereas TDA-DFT captures orbital relaxation only implicitly through the exchange–correlation kernel.[63–66]

An alternative way to include more orbital relaxation in CI methods is to go beyond single-excitation-based methods to correlated methods that include orbital relaxation (perturbatively) *via* doubly (and higher) excited determinants. However, this typically comes at the cost of higher computational demands. In a previous study, some of us applied density functional theory multireference configuration interaction (DFT/MRCI)[67,68] to the STGABS27 benchmark set and found a reasonable agreement for ΔE_{ST} and E_{em} with an error compensation-based approach using the vertical gas phase approximation.[69] One of us also applied correlated wave function methods, namely the algebraic diagrammatic construction method at second order ADC(2), to three selected TADF-emitters, where it shows good agreement with the UKS-based ΔDFT approach.[27] However, so far, no systematic benchmarking of correlated wave function methods has been done on the CT states of TADF-emitters, which is the goal of the present work.

In the following, we give a brief overview of the used methods with a focus on the two main challenges of the STGABS27 set, namely, (i) orbital relaxation effects and (ii) the complete response to the dielectric embedding. Starting off with wave-function-based excited state methods, we employ in this work second-order approximate coupled-cluster singles and doubles (CC2)[70–72] and algebraic diagrammatic construction at second order (ADC(2)).[73–76] Even though these techniques are derived differently, with CC2 being an approximation to the linear-response[77] coupled-cluster method with up to double excitations (CCSD-LR), and ADC(2) being based on the perturbative expansion of the polarization propagator, both are intimately related (*i.e.*, ADC(2) is a symmetrized version of CC2 neglecting singles excitations)[78] and share some crucial advantages compared to other correlated excited state methods: Namely, (i) the scaling of the computational cost with N^5 of the system size N, (ii) the possibility of efficiently avoiding the explicit storage of double excitation amplitudes and other quantities like integral intermediates with N^4-scaling size if combined with the Resolution of the Identity (RI) approximation to reduce the growth of disc space demand to N^3,[78,79] and (iii) their ease of lending themselves to spin-scaling to improve their accuracy.[80] Especially spin-component-scaling (SCS, iii), based on the idea of scaling down the same-spin- and up the opposite-spin-correlation effects as initially proposed for second-order Møller–Plesset Perturbation theory (MP2),[81–83] has shown promise to improve the description of Rydberg- and especially CT-states.[84–86] By completely neglecting opposite-spin correlation in the scaled opposite-spin (SOS) approach, SOS-CC2 and SOS-ADC(2) lend themselves to Laplace transformation to further reduce the scaling of the computational cost to N^4,[87,88] often with similar improvements as the SCS-versions. In combination with the algorithmic improvements (i) and (ii), as well as the development of local-[89] and explicitly-correlated[90] versions, excited state calculations for large molecules become possible.[71,91]

Both ADC(2) and CC2 have been extensively benchmarked in the past for properties such as vertical[16,17,19,21,92–94] and 0-0[95,96] transition energies, potential energy surfaces,[84] and oscillator strengths.[97,98] Where highly accurate reference data is available, the accuracy of excitation energies with both methods is often comparable to CCSD.[99–101] This is the case for the theoretical best estimates in the popular Mühlheim set by Schreiber *et al.*[92] (MUE_{CC2} = 0.30 eV/$MUE_{ADC(2)}$ = 0.29 eV *vs.* $MUE_{EOM\text{-}CCSD}$ = 0.49 eV[102]) and for the even more accurate mountaineering strategy of Loos *et al.* applied to medium-sized organic molecules.[17,94] In line with their close relationship, differences between ADC(2) and CC2 are usually small. However, for Ryberg and especially CT excited states, errors deteriorate substantially with ADC(2) and CC2, which recent studies illustrated for both excitation energies[16] and the excited state potential energy surface.[84] Tajti *et al.* argue that this worse performance compared to valence excitations can be attributed to lacking error-compensation for Rydberg and CT states in the diagonal approximation of the doubles–doubles block made in both CC2 and ADC(2).[103] Spin-scaling approaches can repair the consistent underestimation observed with ADC(2) and CC2 for CT states to some extent.[85,86] While such partially error-compensation-based approaches do not reach the accuracy achieved by the inclusion of (approximate) triples excitations,[104,105] they come at a far lower computational cost.

So far, we only discussed benchmarks for molecules in vacuum derived from gas phase spectroscopy or high-level

theoretical reference methods such as CC3.[106] However, environmental effects can be just as important for predicting experimental results, especially in the present case of polar CT states.[9,27] Because of their computational feasibility and inherent inclusion of sampling effects over the solvent degrees of freedom, continuum solvation models are often a preferred choice over the explicit inclusion of solvent molecules.[40] In contrast to the ground state, excited state calculations face the further complication of two different formalisms for continuum solvation, namely linear-response (LR) and state-specific (SS) solvation, that can yield considerably different results.[107,108] Comparisons of solvatochromism reveal the SS formalism to be generally preferable due to the non-vanishing solvation contribution even in polar CT states, whereas the LR formalism requires a bright transition with a non-zero transition density.[109–111] However, the full SS formalism requires a costly double-iterative optimization of both the excited state reaction field and the ground state wave function. Non-iterative perturbative approximations to the full SS formalism exist (referred to as either ptSS- or cLR-COSMO [for corrected linear-response] in the literature[109,112–114]), but neglect the response of the excited state density to the solvent, which can be crucial for polar CT states (*vide infra*). Thus, while analytical nuclear gradients for iterative SS solvation have become increasingly available,[115–117] it is mainly applied to excited state single-point calculations. This contrasts with state-specific methods such as ROKS/PCM, which enable routine excited state geometry optimization with solvation effects. Yet, few studies actually test high-level electronic structure methods with continuum solvation because accurate experimental reference values are often difficult to obtain. Hence, the highly accurate ΔE_{ST} and E_{em} values of the STGABS27 set, which are obtained from temperature-dependent measurements in solution, provide a rare and insightful challenge.

II. Approach and methodology

For our investigation, we split the STGABS27(-EMS) into two subsets based on the size of the emitters (A: 1–9, 11, 14, 15, 24, and 27; (B) the remainder, see Fig. 1). This allows us to compare various computationally demanding method combinations (*i.e.*, larger basis sets) on subset A (up to 81 atoms) without requiring calculations for the larger systems in subset B (up to 139 atoms). Unless stated otherwise, we treat singlet–triplet gaps adiabatically at the excited state geometries and emission energies vertically at the S_1 geometry, following the Franck–Condon approximation.[118,119] We use the geometries provided in ref. 30 for S_1 and T_1 optimized with ROKS/UKS/PCM and the optimally-tuned RSH-functional LC-ωPBE (OT-LC-ωPBE) and for the ground state optimized with the PBEh-3c composite

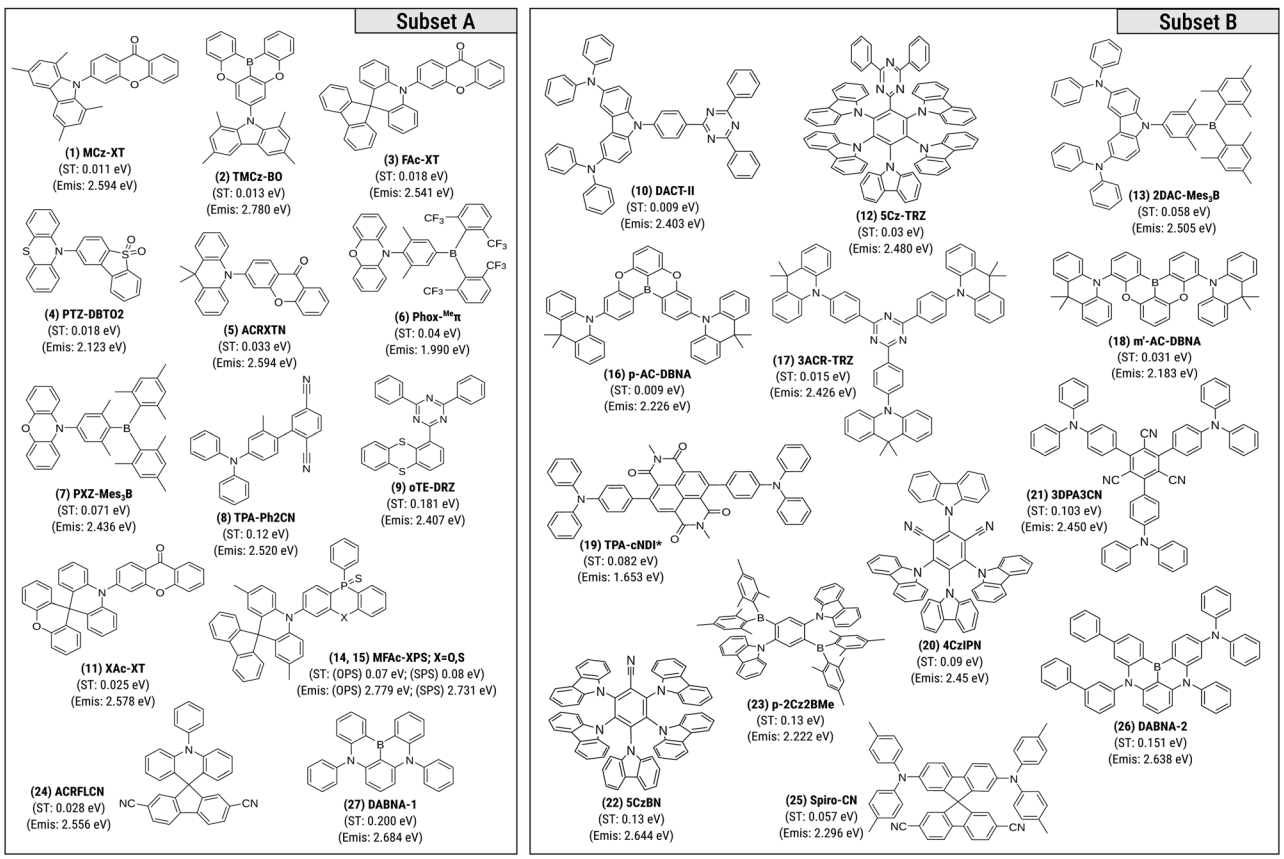

Fig. 1 Overview of molecular structures included in the STGABS27 benchmark set. Systems are divided into two subsets A and B according to their molecular size.

method.[120] This circumvents the need for method-specific geometry optimization, which remains unfeasible at this system size even with the recently introduced analytical gradients of state-specific solvation models for approximate second-order methods due to the costly triple-iterative procedure (geometry optimization, reaction field equilibration, and SCF).[117]

All calculations with the ADC(2) and CC2 methods were carried out with the ricc2 module[78,79,121–124] in a development version of the Turbomole program,[125–127] which includes state-specific solvation models for CC2.[117,128] Aside from the canonical form of ADC(2) and CC2, also the spin-component-scaled (SCS, 33% same-spin and 120% opposite-spin) and scaled opposite-spin (SOS, 0% same-spin and 130% opposite-spin) versions were tested with standard scaling parameters. To model the effect of the dielectric environment, we employed the conductor-like screening model (COSMO).[40,129–133] Because the excited states in question exhibit almost exclusively strong CT character, COSMO was preferentially applied in the difference-density-based state-specific formalism,[48,55,107,134–140] either fully self-consistently (denoted SS-COSMO or PerTurbation of Energy and Density (PTED) in the literature)[110,116,117,128,141] or in perturbative approximation (referred to as either ptSS- or cLR-COSMO [for corrected linear-response] in the literature[109,112–114,142]). The transition-density-based linear-response formalism[143,144] was only used in exploratory calculations, either combined with iterative SS-COSMO (SS + LR-COSMO) or on its own in the form of the post-SCF-COSMO[111,145] model. Due to their long lifetimes in TADF emitters, both singlet and triplet excited states were treated within the regime of equilibrium solvation governed by the static dielectric constant ε. As suggested in ref. 30 and 55, ε was set to the global value of 3.0 in all calculations of ΔE_{ST} as an intermediate value between toluene (ε = 2.37) and more polar thin-film matrices. Meanwhile, the final ground state after the fast emission process is modeled in the regime of non-equilibrium solvation governed by the refractive index n.[146–149] Here, measurement-specific values for ε and n were used.[48]

In light of the substantial size of some emitters and the double-iterative procedure of ADC(2) and CC2 with SS-COSMO, most calculations had to be limited to the small def2-SVP basis set.[150–152] Since the basis set incompleteness error (BSIE) will be substantial at the double-ζ level, we employed the larger def2-TZVPP basis set for subset A of smaller molecules.[151] To make this possible, only the final excited-state calculation in the reaction field converged with def2-SVP uses the def2-TZVPP basis set. While there might be minor incompatibilities between the def2-SVP and a fully converged def2-TZVPP reaction field, similar schemes (*i.e.* use of an ADC(2) reaction field for a final ADC(3)[102] calculation) showed that energetic errors are often small.[110]

III. Results and discussion

A. Second-order excited state methods

Let us begin the analysis of the second-order methods with their performance for singlet–triplet gaps. To separate the crucial role of the electronic structure method from the choice of the excited state solvation model, we initially limit the discussion to results with fully self-consistent SS-COSMO. Fig. 2 depicts ΔE_{ST} values for all emitters in the STGABS27 with ADC(2) and its spin-scaled versions, while Fig. 4b plots the associated statistical error distributions as boxplots. For comparison, we also show the most accurate orbital-optimized state-specific ΔDFT results on the STGABS27,[30] specifically ROKS/PCM with OT-ωB97M-V functional in green, in addition to the experimental values in black.

The most striking result is the excellent agreement between the experiment and spin-component scaled SCS-ADC(2) (red). With a mean unsigned error (MUE) of 0.035 eV and a standard deviation (SD) of 0.044 eV, SCS-ADC(2) exhibits the smallest errors of all tested second-order methods and is only outperformed by state-specific approaches such as ROKS/PCM (MUE of 0.022 eV). Most gaps are within (17) or close to (8) chemical accuracy defined by 1 kcal mol^{-1} error w.r.t. the reference ($\approx$0.05 eV, grey band). Moreover, no substantially negative ST-gaps occur, as is expected for the predominantly singly-excited CT states.[61,153] Instead, the error distribution centers close to zero with a vanishing mean signed error (MSE) of 0.004 eV. Notably, SCS-ADC(2) also shows a remarkable agreement with ROKS/PCM (relative MUE of 0.023 eV between both methods). Even in cases where both methods deviate from the experiment, they usually do so in the same direction. This might in part be a result of using the ROKS/PCM excited-state geometries for ADC(2) and CC2 calculations. While for 18 of the 27 emitters, SCS-ADC(2) and ROKS agree to within 0.02 eV, there are few cases with slightly larger deviations of $\approx$0.05 eV (9, 21, 26, 27), and only one case with a deviation $>$0.1 eV (for SCS-ADC(2), canonical ADC(2) and ROKS are spot-on). This maximum deviation is observed for TPA-Ph2CN (molecule 8), which appears to be particularly challenging, as previously pointed out by Kaminski *et al.* using DFT/MRCI (see SI and the discussion below for further details).[69,154]

Generally, the excellent agreement is particularly remarkable given the fundamentally different nature of the CI-based SCS-ADC(2) with iterative SS-COSMO and the state-specific orbital-optimized ROKS/PCM or UKS/PCM using basically a ground-state solvent model. Both methods outclass the best-performing TDA-DFT-based approaches (light and dark blue in Fig. 4b), cutting the error spread by almost an order of magnitude. Moreover, their close correlation with each other and the experimental references confirm the assumptions made in the interpretation of the experimental data, *i.e.*, the adiabatic nature of the gaps and the singlet–triplet gap as the limiting factor for the temperature-dependent TADF rate. Hence, relaxed (ROKS/PCM optimized) excited state structures are essential for this level of accuracy. In comparison, vertical gaps calculated at the ground state geometry tend to be mostly zero in predictions with both methods (*vide infra* and SI for more details).

Comparing now SCS-ADC(2) with the canonical (purple) and scaled opposite-spin (orange) versions, a clear trend emerges: with decreasing/increasing same/opposite-spin correlation, the

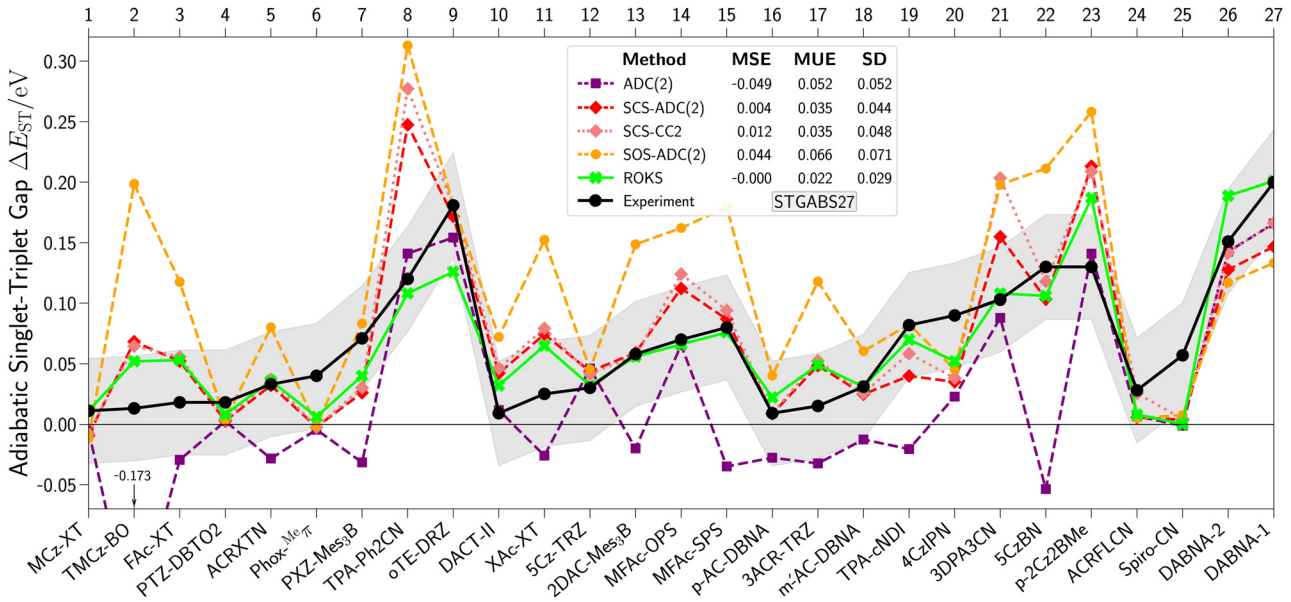

Fig. 2 Experimental (black) and calculated singlet–triplet gaps ΔE_{ST} for the emitters of the STGABS27 benchmark set. The calculated values are given for canonical (purple), spin-component-scaled (SCS, red), and scaled opposite-spin (SOS, orange) ADC(2), as well as SCS-CC2 (light red). All calculations employ fully iterative SS-COSMO solvation, the split-valence def2-SVP basis set, the UKS/ROKS/PCM optimized S_1/T_1 geometries with the OT-LC-ωPBE functional from ref. 30, and a dielectric constant of ε = 3.0. Connecting lines between individual datapoints serve only to guide the readers eye. The target error margin corresponding to chemical accuracy ($\approx\pm$0.05 eV) is marked by a grey band around the experimental values. For comparison, the most accurate ROKS/PCM-based method with OT-ωB97M-V and the def2-SVP basis set is depicted in green. MSE, MUE, and SD values for the complete STGABS27 set are tabulated.

gaps progress from too small or even negative values with canonical ADC(2) (MSE: −0.049 eV) to sometimes a substantial overestimation with SOS-ADC(2) (MSE: 0.044 eV). Curiously, the only exceptions are the MR-TADF emitters DABNA-1/2 (26 and 27), where differences are much smaller and inverse. The reason for this behavior is the stabilizing effect of same-spin correlation on CT relative to locally excited (LE) states, which opposes the inverse effect of (same-spin) Fock exchange in ADC(1) (equivalent to CIS).[55,66] Exchange integrals over both the electron and hole wavefunction give rise to their attractive interaction in ADC(1), leading to a general overestimation of CT excitation energies. This Coulomb interaction is (over-)screened by second-order orbital-relaxation terms that are folded into the singles block in ADC(2), which leads to overly polarized CT states.[155] Since the S_1 is generally the more polar state with stronger CT character,[27] its excitation energy with canonical ADC(2) can approach or even move below the T_1 state, which results in many artificially inverted gaps (mols. 2, 3, 5, 7, 11, 13, 15–19).[85,92] In contrast, the complete neglect of same-spin correlation along with the up-scaled opposite-spin correlation in SOS-ADC(2) leads to an apparent underestimation of orbital-relaxation effects and, in turn, an overestimation of the energy for CT relative to LE states. Together, these effects cause the ST-gaps to be substantially too large with SOS-ADC(2), as evident from the positive MSE of 0.044 eV. This overall trend is particularly apparent in systems such as TMCz-BO (2), ACRXTN (5), TPA-Ph2CN (8), and 5CzBN (22), where the T_1 state changes from a strong CT state with canonical ADC(2) to a mixture with a local excitation in SOS-ADC(2) (see SI for details). In contrast, systems where the CT character of both states is locked-in, such as PTZ-DBTO2 (4), Phox-$^{Me}\pi$ (6), or where donor and acceptor are forced to orthogonality, like the sterically crowded 5Cz-TRZ or the spiro-compounds ACRFLCN (24) and Spiro-CN (25), yield almost no difference between the scaled and canonical ADC(2). Evidently, for a balanced description of LE and CT states, same- and opposite-spin terms are important, and the down-scaled same-spin- of 33% and up-scaled opposite-spin-contribution of 120% for SCS-ADC(2) is the sweet spot for the molecules in the STGABS27 set, at least with the efficient def2-SVP basis set.

Before moving on, we should discuss the non-negligible impact of using a larger def2-TZVPP basis set compared to def2-SVP, for which most results are presented. Because of the steep computational cost of the second-order methods with def2-TZVPP, we could only sample this effect for subset A of smaller emitters and only used the larger basis in the final SS-COSMO iteration, *i.e.*, with a solvent field optimized for def2-SVP. The triple-ζ def2-TZVPP systematically lowers both the singlet–triplet gaps ($\approx$0.05 eV) and the vertical emission energies ($\approx$0.15 eV, *vide infra*) across the STGABS27 set, as evident from Fig. 3. Since the magnitude of the def2-TZVPP shift is far larger for ADC(2) and CC2 than the $\lesssim$0.02 eV basis-set sensitivity we observed for orbital-optimized state-specific ΔDFT approaches such as ROKS/PCM,[30,48] it is no longer negligible. While the basis set choice significantly impacts the agreement with the experiment, the effect is very systematic, which allows us to generalize. Qualitatively, the down-shift nudges SCS-ADC(2) away from its sweet spot: gaps that were almost spot-

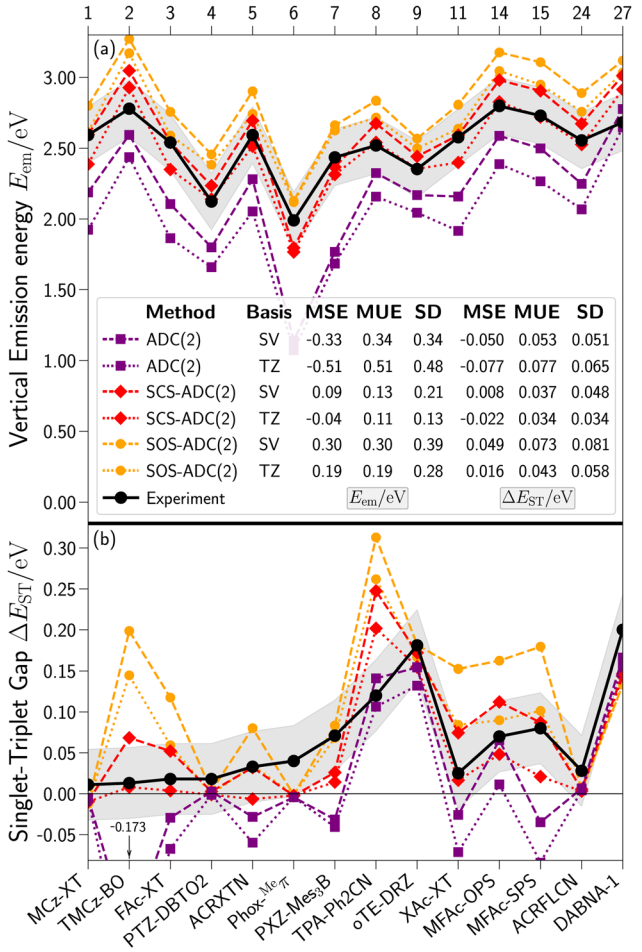

Fig. 3 Experimental (black) and calculated (a) emission energies E_{em} and (b) singlet–triplet gaps ΔE_{ST} for subset A of the STGABS27 benchmark set. The calculated values are given for canonical (purple), spin-component-scaled (SCS, red), and scaled opposite-spin (SOS, orange) ADC(2) with fully iterative (pt)SS-COSMO solvation, including perturbative corrections for emission. Results are presented either always with the small split-valence def2-SVP (SV, dashed) basis set or with the larger triple-ζ def2-TZVPP (TZ, dotted) basis set for the final solvent field equilibration step. All calculations employ the UKS/ROKS/PCM optimized S_1/T_1 geometries with the OT-LC-ωPBE functional from ref. 30, and either a dielectric constant of ε = 3.0 for singlet–triplet gaps or system-specific values for ε and the refractive index n dependent on the experimental measurement for emission energies. Connecting lines between individual datapoints serve only to guide the readers eye. The target error margin corresponding to chemical accuracy ($\approx\pm$0.05 eV) for ΔE_{ST} and conservative experimental errors of $\pm$0.2 eV for the E_{em} are marked by grey bands around the experimental values. MSE, MUE, and SD values for subset A of the STGABS27 are tabulated.

on with def2-SVP now become slightly underestimated, as evident from the MSE moving from 0.008 eV (def2-SVP) to −0.022 eV (def2-TZVPP) for subset A, while the performance (MUE) hardly changes (*cf.* inlay Fig. 3). Conversely, SOS-ADC(2), which appears to overshoot with def2-SVP, benefits from the larger basis and moves noticeably closer to the experiment, as evident from the MSE (0.049 eV to 0.013 eV), MUE (almost halved from 0.073 eV to 0.043 eV), and SD (0.081 eV to 0.058 eV). For canonical ADC(2), the systematic underestimation becomes even worse with def2-TZVPP (MSE = MUE from −0.050 eV to −0.077 eV). Overall, taking a pragmatic viewpoint, we focus our discussion on calculations with the more efficient def2-SVP basis sets since the minor improvements in MUE and SD hardly justify the huge increase in computational cost. From this perspective, SCS-ADC(2)/def2-SVP should be preferred, also because it achieves a lower SD than the SOS variant in every combination. However, when extrapolating to the complete basis set limit, the underestimation by SCS- and overestimation by SOS-ADC(2) appear to balance. This is most evident perhaps for the emission energies discussed further below, where the systematic overestimation of SOS-ADC(2)/ptSS-COSMO/def2-TZVPP compared to the experiment is in line with the neglect of vibronic effects.[48,157–159] Also, the availability of reduced scaling implementations based on the Laplace transform and recent tensor hypercontraction (THC) techniques favor SOS-ADC(2).[88,160] Nevertheless, SCS-ADC(2) consistently achieves a significantly lower SD (even with def2-SVP compared to SOS-ADC(2)/def2-TZVPP), hinting that including same-spin integrals improves the description of CT states and cannot fully be compensated by simply upscaling the opposite-spin contributions.

Having established the performance of ADC(2) and variants, let us move to the closely related second-order approximate coupled cluster, CC2. While ADC(2) and CC2 typically agree to within 0.1 eV, mixing between the ground and low-lying singly excited states moderated by the singles amplitudes in CC2 can lead to discrepancies in cases with particularly low excited states and/or LUMO energies.[161,162] Fig. 4b displays the statistical distributions (shaded), while Fig. 2 compares the best-performing SCS-ADC(2) and SCS-CC2 (all other variants are shown in Fig. S1 in the SI). Comparing the error distribution for the equivalently spin-scaled ADC(2) and CC2 versions, we observe only a minor increase of $\approx$0.008 eV in the MSE and almost unchanged statistical deviations. Differences between ADC(2) and CC2 appear for a few systems (8, 19, 21), but the increase of ΔE_{ST} remains below 0.05 eV (see Fig. 2 and Fig. S3 in the SI). Notably, the largest shift occurs not for TPA-cNDI* (19), the system with the lowest emission energy by far (*vide infra*) and thus expected to be most susceptible to state-mixing between ground and S_1 states.[161] Instead, 3DPA3CN (21) and TDA-Ph2CN (8) with rather average E_{em} show larger deviations between ADC(2) and CC2. For these two cases, the gaps are systematically overestimated by (SCS-)CC2, such that the smaller gaps of (SCS-)ADC(2) are closer to the experimental references. Only for TPA-cNDI*, (SCS-)CC2 is closer to the experiment. While there are too few molecules and too small effects to arrive at any meaningful conclusions here, we want to mention that in a recent work, Sülzner *et al.* argued that the single excitations in CC2 become important mainly in the description of low-lying excited states.[161]

The performance for vertical emission energies E_{em} in the STGABS27-EMS set offers a great opportunity to cross-check the conclusions drawn on the adiabatic singlet–triplet gaps. As discussed extensively in ref. 48, uncertainties for experimental E_{em} values are substantially larger (conservative error range of $\pm$0.2 eV, grey band) than for ΔE_{ST}. The main reasons

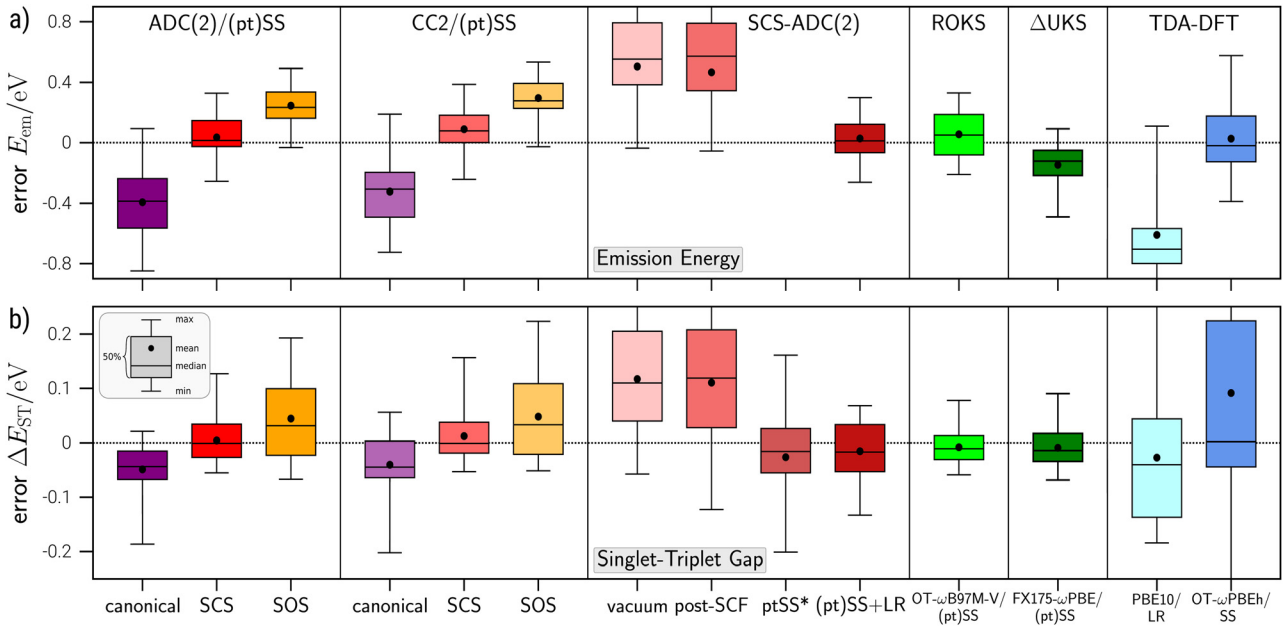

Fig. 4 Deviations for (a) the vertical emission energies E_{em} and (b) adiabatic singlet–triplet gaps ΔE_{ST}. Results are shown for canonical (purple), spin-component-scaled (SCS, red), and scaled opposite-spin (SOS, orange) ADC(2) and CC2 (shaded) with the fully iterative (pt)SS-COSMO including perturbative corrections for emission. Values with SCS-ADC(2) and different solvent models are shown in the middle (shaded red). For comparison, results for ROKS/(pt)SS-PCM with OT-ωB97M-V (light green), ΔUKS/(pt)SS-PCM with FX175-ωPBE (dark green), as well as TDA-DFT/LR-PCM with PBE10 (light blue) and TDA/SS-PCM with OT-LRC-wPBEh[156] (dark blue) are depicted on the right. All calculations employ the UKS/ROKS/PCM optimized S_1/T_1 geometries with the OT-LC-ωPBE functional from ref. 30 and the def2-SVP basis set.

are deviations from the ideal Franck–Condon behavior during the transition and the prominent vibrational line broadening of CT fluorescence peaks. Still, E_{em} complement the highly accurate gaps between the very similar singlet and triplet CT states well by sampling the energy difference between the polar excited and unpolar ground states and emphasizing the treatment of solvation effects. Initially, we restrict the discussion to calculations using ptSS-COSMO with non-equilibrium relaxation of the final ground state as the appropriate continuum solvation model for vertical transitions out of polar CT states (*vide infra*, see SI for details). Fig. 4a plots the error distribution, and Fig. 5 the explicit emission energies for all systems with (spin-scaled) ADC(2) and SCS-CC2.

Beginning with the best-performing method for ΔE_{ST}, we observe again excellent agreement between SCS-ADC(2) and the experimental reference values. The error distribution is narrow (SD: 0.15 eV) and centered around zero (MSE: 0.04 eV), which is further improved with the larger def2-TZVPP basis set (see Fig. 3a). However, the absolute error spread increases by a factor of 3–4 compared to ΔE_{ST} (MUE: 0.12 *vs.* 0.035 eV). We rationalize this with the aforementioned larger differences between the initial (singlet CT) and final (singlet ground) states, which reduces beneficial error cancelation compared to ΔE_{ST}. Still, only a few predictions fall outside of the larger experimental error margins for E_{em} (6 out of 27). As for ΔE_{ST}, the predicted E_{em} values with SCS-ADC(2) and ROKS/PCM (also UKS/PCM, not shown) match closely with a relative MUE of 0.10 eV and deviations below 0.1 eV for 15 out of 27 systems.

Given the excellent performance of both approaches for different properties, their relative deviation offers valuable insights. Systems for which SCS-ADC(2) predicts significantly lower emission energies than ROKS/PCM (4, 6, and 12) exhibit strong CT, typically with large electron–hole separation and high dipole moments. Such cases with strongly dominant CT character in S_1 and T_1 are generally simpler (no balancing with LE states is needed). Accordingly, we observe only insignificant differences between (SCS)-ADC(2) and ROKS for the singlet–triplet gaps. In contrast, if SCS-ADC(2) predicts higher E_{em} than ROKS, as is the case for mols. 8, 9, and 23, the respective states tend to be less polar with mixed LE/CT character in the triplet. However, it bears pointing out that the differences mostly vanish when considering the SCS-ADC(2) results obtained with the larger basis sets (available for 8 and 9 in Fig. 3), at least for the emission energies. Regarding both the singlet–triplet gaps and emission energies, TPA-Ph2CN (8) remains a challenging example for SCS-ADC(2), whereas ROKS/PCM offers an almost perfect agreement for both experimental ΔE_{ST} and E_{em}. In this case, it appears that SCS-ADC(2) yields too unpolar states, which explains the overestimation of the singlet–triplet gap and emission energy.

In summary, the ADC(2) results for the emission energies mostly confirm our conclusions from the singlet–triplet gaps: canonical ADC(2) clearly underestimates, SOS-ADC(2) slightly overestimates, while SCS-ADC(2) provides a balanced description, at least with the small def2-SVP basis set (the same holds for SCS-CC2, see Fig. S2 in the SI for details). With the larger def2-TZVPP basis set for the final solvent field equilibration step, the emission energies decrease substantially, moving SOS-ADC(2) closer to the experiment (MSE for the subset A from

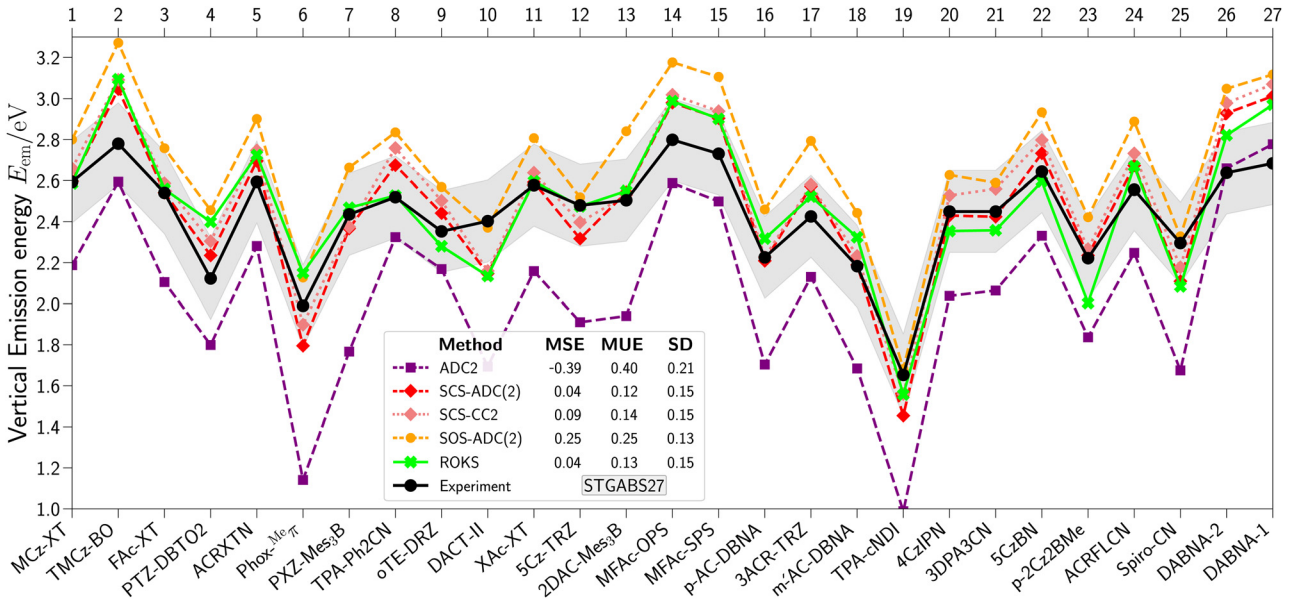

Fig. 5 Experimental (black) and calculated emission energies E_{em} for the emitters of the STGABS27 benchmark set. The calculated values are given for canonical (purple), spin-component-scaled (SCS, red), and scaled opposite-spin (SOS, orange) ADC(2), as well as SCS-CC2 (light red). All calculations employ fully iterative ptSS-COSMO solvation with perturbative corrections, the split-valence def2-SVP basis set, ROKS/PCM optimized S_1 geometries with the OT-LC-ωPBE functional from ref. 30, and system-specific values for the dielectric constant ε and the refractive index n dependent on the experimental measurement. For comparison, emission energies with ROKS/ptSS-PCM with OT-ωB97M-V and the def2-SVP basis set are depicted in green. Connecting lines between individual datapoints serve only to guide the readers eye. The conservative experimental error margin of $\pm$0.2 eV is marked by a grey band around the experimental values. MSE, MUE, and SD values for the complete STGABS27 set are tabulated.

0.16 eV to 0.10 eV), while SCS-ADC(2) very slightly underestimates the emission energies (MSE for subset A from 0.05 eV to −0.02 eV) with the larger basis set. Systems 26 and 27 break with the general trend as ADC(2) is better, also for the gaps. The reason is that instead of long-range CT in classical donor–acceptor systems, multi-resonance TADF emitters exhibit short-range CT (SRCT) states, where doubly-excited determinants are more important than orbital-relaxation effects.[62] CC2 and ADC(2) and their respective variants are again very similar with only three differences larger than 0.1 eV (for SCS 6, 19, and 21 while 11 is just below) and most differences on the order of 0.05 eV. The differences are always largest between the canonical variants and in all, but one case (2DAC-Mes$_3$B, 13), the CC2 excitation energies are larger than those obtained with ADC(2). Finally, we note that ROKS/PCM is again very similar to SCS-ADC(2)/SS-COSMO with few small deviations (*vide supra*) and virtually identical statistics (MSE both 0.04 eV, MUE 0.12/0.13 eV). It should be noted that for the emission energies, a very similar performance can be obtained with unrestricted Kohn–Sham (UKS)/PCM using LC-ωPBE-D4 with a range-separation parameter of 0.200 a.u. The advantage over ROKS is that UKS is more robust and also works for INVEST and MR-TADF emitters, where ROKS fails.[48,61,62]

B. Solvation models

Having established that the SCS- and SOS-variants of ADC(2) and CC2 accurately describe ST gaps and emission energies with the full iterative state-specific solvent model, we now take an in-depth look at the various (approximate) excited state solvation models. Fig. 6 displays the singlet–triplet gaps of subset A obtained with SCS-ADC(2) in combination with a variety of both linear-response and state-specific solvation models as well as in gas phase (see Fig. S4 for the full STGABS27 set). Most importantly, the results in gas phase (green) strikingly illustrate the necessity of including dielectric embedding to obtain any reasonable estimate for ΔE_{ST}. Without any dielectric environment (green), the gaps are much too large, which results from an imbalanced treatment of (mostly singlet) CT and (mostly triplet) LE states. This picture hardly changes with the post-SCF-COSMO approach (blue), which derives from the linear-response formalism. The underlying reason is the well-known failure of the transition-density-based LR-approach for polar CT states (and triplets) due to their vanishing transition density.[30,55] With few exceptions (*vide infra*), the post-SCF COMSO results are thus equivalent to using solvated ground state orbitals, which evidently lack any stabilization for the charge-separated excited states. Accordingly, not only energies but also the characters of the low-lying states are as wrong in the gas phase as with post-SCF-COSMO, where most triplets and even some singlets wrongly come out as LE states. Even for the two exceptions where the linear-response contribution is not negligible, namely the SRCT states of the MR-TADF emitters DABNA-1/2 (26/27), the LR-COSMO contribution is unbalanced as it only stabilizes singlets but not triplets. Consequently, the combined iterative SS + LR-COSMO (purple), which accurately recovers state orderings and characters, also does not improve the results for molecules with bright transitions (mainly 26 and 27) compared to the pure SS-COSMO. The unbalanced

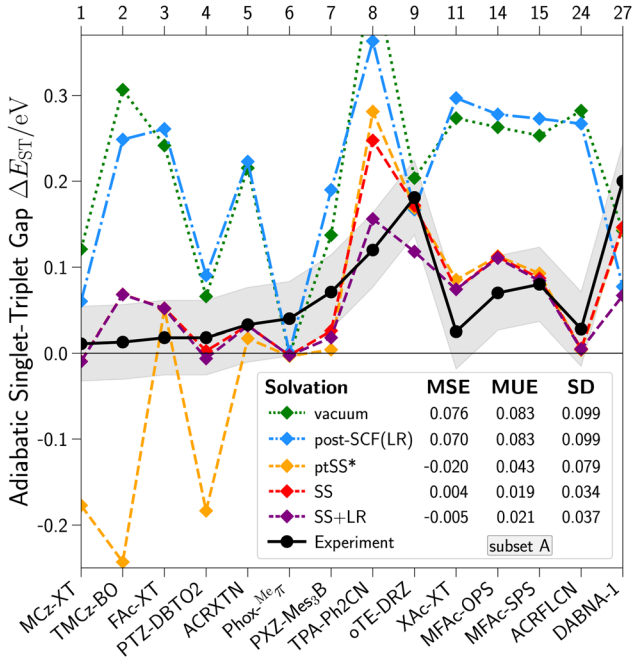

Fig. 6 Experimental (black) and calculated singlet–triplet gaps ΔE_{ST} for the subset A of the STGABS27 benchmark set. The calculated values are given for SCS-ADC(2) with different models for the environment: vacuum (green), linear-response-based post-SCF-COSMO (blue), perturbative equilibrium state-specific (ptSS*-)COSMO (orange), full iterative SS-COSMO (red), and full iterative SS-COSMO with added linear-response solvation (SS + LR, purple). All calculations employ the UKS/ROKS/PCM optimized geometries with the OT-LC-ωPBE functional from ref. 30, a dielectric constant of ε = 3.0, and a def2-SVP basis set. Connecting lines between individual datapoints serve only to guide the readers eye. The target error margin corresponding to chemical accuracy ($\approx\pm$0.05 eV) is marked by a grey band around the experimental values. MSE, MUE, and SD values for subset A of the STGABS27 set are tabulated.

LR-stabilization of the S_1 state helps only for TPA-Ph2CN (8), where SCS-ADC(2) generally struggles (*vide supra*). Thus, we conclude that any linear-response-derived solvent model should be avoided.

One of the main drawbacks of the state-specific solvent model is the high computational cost of iterative solvent-field optimization (essentially a geometry optimization for the implicit solvent). To remedy this, we use the perturbative approximation to state-specific solvation (denoted ptSS*-COSMO, yellow), which is commonly applied in a non-equilibrium formalism for vertical transitions (*e.g.*, in the calculation of emission energies with ptSS-COSMO, also denoted cLR-COSMO in literature).[109,142] To calculate the ptSS* correction for equilibrium solvation, we just replace the squared refractive index n^2 with the dielectric constant ε (see the SI for technical details). As some of us have shown before on artificial CT model systems, this perturbative equilibrium solvation can mimic the full self-consistent approach as long as the solvent field does not significantly alter the state character (changes in the state-ordering are not an issue, as one can simply reorder the states after adding the correction).[109,110] The results for STGABS27 confirm this: ptSS* and full SS-COSMO closely agree for most systems with deviations below 0.05 eV. Only MCz-XT (1), TMCz-Bo (2), and PTZ-DBTO2 (4) show larger deviations because of the aforementioned issue with state characters. In these emitters, the T_1 and T_2 are roughly equal mixtures of LE and CT contributions in the ground state solvent field, such that neither of them receives the full dielectric stabilization in the one-shot calculation with the ptSS* approximation. However, just one additional excited-state calculation in the polarized state-specific solvent field of the CT state helps to disentangle the state characters, creating a CT-dominated triplet state and restoring the singlet–triplet gap. Since this is still much cheaper than fully converging the solvent field in typically 5–10 iterations, we suggest this mixed 2-step-SS/ptSS approach as an efficient alternative.

C. Geometry

Finally, we explore the effect of the geometry used in the calculations and compare the optimized S_1 and T_1 excited state geometries with the ground state geometry. While a consistent optimization at the SCS-ADC(2)/SS-COSMO level poses a prohibitive computational expense even with the recently developed analytical gradients,[117] ROKS/PCM and UKS/PCM can efficiently provide excited state structures with full account of solvation effects.[30] Fig. 7 compares singlet–triplet gaps (a) and emission energies (b) obtained with SCS-ADC(2)/SS-COSMO and ROKS/PCM for either excited-state optimized structures (S_1/T_1) from ROKS/UKS/PCM or ground-state optimized structures (GS) obtained with PBEh-3c. Comparing the different approaches for emission energies shows that, unsurprisingly, emission energies calculated for GS geometries in the gas phase (otherwise called absorption energies) are strongly and systematically blue-shifted (dotted blue, MSE 1.23 eV). Interestingly, the statistical evaluation of the "mixed" SCS-ADC(2) results for GS structures with state-specific solvation (dotted red, MSE 0.70 eV) and for S_1 structures without solvation (dashed blue, MSE 0.63 eV) reveals that relaxation of the solute geometry and the solvent field contribute equal parts to the total Stokes shift. In fact, there are only two molecules (4 and 9) where the solute geometry clearly dominates, while all other cases, especially 2 and 5, show a larger impact of the solvent field. The relative size of the contributions can be rationalized by thinking of the solvent-field iterations as geometry optimization for the implicit solvent. This result underlines yet again how important solvation effects are for these molecules, even in the relatively non-polar environments assumed here (ε = 3).

Moving now to the ST gaps shown in Fig. 7b, the solvent model is much more important than using excited state structures. While ground-state structures with SCS-ADC(2)/SS-COSMO afford a good MUE of 0.051 eV, excited-state structures and gas-phase SCS-ADC(2) increase the MUE to 0.160 eV. Similarly, ROKS with GS structures is almost as accurate (MUE 0.030 eV) as with S_1/T_1 structures (MUE 0.021 eV). At the ground state structure, predicted gaps decrease in most cases (MSE from 0.008 to −0.016 for SCS-ADC(2)/SS-COSMO), which is in large part due to the more orthogonal donor–acceptor arrangement, reducing destabilizing exchange for

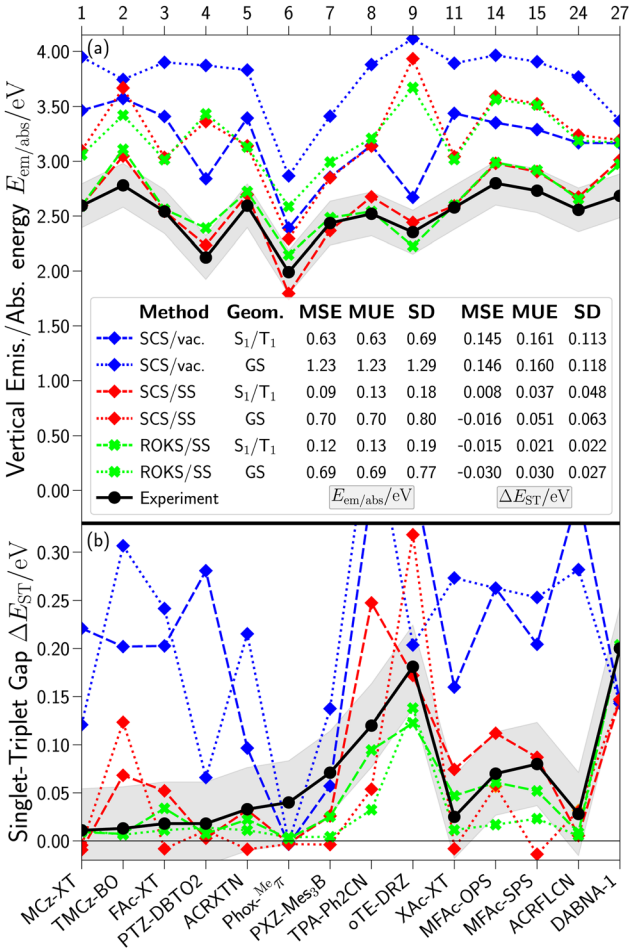

Fig. 7 Experimental (black) and calculated emission energies E_{em} (a) and singlet–triplet gaps ΔE_{ST} (b) for subset A of the STGABS27 benchmark set. The calculated values are given either at the excited state (S_1/T_1) geometries optimized with UKS/ROKS/PCM using the OT-LC-ωPBE functional (dashed lines) or at the ground state (GS) geometries optimized with PBEh-3c (dotted lines) from ref. 30. Results are shown for SCS-ADC(2)/vacuum (blue), SCS-ADC(2)/SS-COSMO (red), and ROKS/PCM (green) with the OT-ωB97M-V functional all using the def2-SVP basis set. All calculations of ΔE_{ST} employ a dielectric constant of ε = 3.0, while calculations of E_{em} employ system-specific values for ε and the refractive index n dependent on the experimental measurement. Connecting lines between individual datapoints serve only to guide the readers eye. The target error margin corresponding to chemical accuracy ($\approx \pm 0.05$ eV) for ΔE_{ST} and conservative experimental errors of ± 0.2 eV for the E_{em} is marked by grey bands around the experimental values. MSE and MUE values for subset A of the STGABS27 are tabulated.

the singlet state.[55] This is consistent with previous reports that ST gaps can be estimated reasonably well in the vertical (or Franck–Condon) approximation for all kinds of TADF emitters.[30,62,69] Despite the reasonable agreement of SCS-ADC(2) and ROKS in the vertical approximation, the results show that relaxed excited state structures obtained with ROKS/UKS significantly and consistently improve the agreement (MUE 0.037 eV and SD from 0.063 eV to 0.041 eV) at the SCS-ADC(2) level of theory. Note that this is in stark contrast with TDA-DFT and, to a lesser extent, DFT/MRCI results, where ROKS/UKS optimized excited-state structures yield much worse estimates for the ST-gaps than the GS geometry.[55,69] The effect has been traced back to the deviation of the ROKS/UKS/PCM geometries from a strict 90° dihedral angle between the donor and acceptor subunits in the TADF emitters. The substantial errors for different structures along the donor–acceptor dihedral angles hint at a systematic issue of TD-DFT with twisted intramolecular CT structures, even when optimally tuned RSHs are used. Overall, these results nicely demonstrate that ROKS/UKS/PCM geometries can serve as a computationally inexpensive alternative for conducting excited state optimizations with correlated methods, which affords the full inclusion of equilibrium solvation effects.

IV. Summary and conclusions

We presented an investigation into the performance of second-order correlated wavefunction methods for the description of the strong CT states in solution contained in the TADF-emitter benchmark set STGABS27. Based on the accurate experimental references for both singlet–triplet gaps and emission energies, we explore four major variables in the calculation of CT states, namely, (i) the electronic structure itself in the form of different spin-scaling schemes for the second-order methods, (ii) the basis-set dependency, (iii) the description of the dielectric embedding with continuum solvation models, and (iv) the choice of the molecular structure. With this investigation, we complement the recent findings that firstly, ΔDFT methods afford unprecedented accuracy for both ΔE_{ST} and E_{em}, and secondly, TDA-DFT requires a trade-off between accurately calculating ΔE_{ST} or E_{em}.

The results established that the best-performing second-order methods for singlet–triplet gaps and emission energies are the spin-component-scaled or scaled opposite-spin variants of ADC(2) or CC2 in combination with iterative and state-specific SS-COSMO at the adiabatic, ROKS/UKS/PCM optimized excited state geometries. While ADC(2) and CC2 are approximately equal, spin-scaled variants are a substantial improvement as they mitigate the severe over-stabilization of CT states with canonical ADC(2)/CC2.[86] Depending on the basis set, either SCS (def2-SVP) or SOS (def2-TZVPP) provides the lowest mean absolute error from experimental data. However, when focusing on the reproduction of trends rather than absolute values as reflected in the standard deviation (SD), the inclusion of same-spin contributions gives the SCS variant a distinct edge over SOS-ADC(2), irrespective of which basis set is used. Regarding the solvation effects, the iterative SS-COSMO model is the most accurate, while the perturbative ptSS* variant can help to reduce the number of solvent field iterations with a small loss in accuracy. In contrast to SS-solvation, linear-response-based methods completely miss the dielectric stabilization of CT states and yield poor results, and even worsen the overall performance when combined with the iterative SS-COSMO approach. Generally, for accurate ST-gaps, we found that solvation effects are more important than geometric

relaxation, while both are equally important (and required) for accurate emission energies.

Considering previous results for STGABS27 with (orbital-optimized) ΔDFT methods like ROKS/PCM (MUE 0.022 eV for ST gaps) and UKS/PCM, it bears pointing out that spin-scaled ADC(2)/CC2 show remarkable agreement with ΔDFT. Despite their fundamentally different nature, SCS-ADC(2)/CC2 and ROKS/UKS/PCM closely agree with each other for gaps and emission energies (*cf.* Fig. 2 and 5). As a result, the MUE between these orthogonal theoretical approaches is only 0.025 eV for ST-gaps and thus smaller than the deviation between SCS-ADC(2)/SS-COSMO and the experiment. This nicely shows that it is possible to reproduce experimental data with sub-kcal mol^{-1} accuracy (for ST gaps) with different methods if all the physics (geometric relaxation, dielectric stabilization, orbital relaxation) is modeled in a balanced way, irrespective if excitation-based methods like CC2/ADC(2) or ΔDFT are employed. By far the biggest difference between the methods lies in their computational effort, where ΔDFT methods are about two orders of magnitude faster than equally accurate second-order excitation-based methods.

Overall, we conclude that this investigation of second-order methods nicely demonstrates the intricacies of describing charge transfer in a dielectric environment and how the reference data from the STGABS27 set can be utilized for a deeper understanding. First off, the close consensus on the size of the singlet–triplet gaps between theory at different levels and the experiment validates not only the choice of theoretical method but also the experimental procedure. If assumptions such as that the (r)ISC occurs between equilibrated excited states or that the fluorescence rate is approximately temperature-independent would not hold, the simple assumption of calculating both states adiabatically would produce disagreements. Hence, the STGABS27 set, specifically its highly accurate singlet–triplet gaps, is a unique collection of benchmark-quality reference values to test the description of CT states in solution, even for high-quality correlated wavefunction theory. Secondly, the agreement between SCS-ADC(2)/SS-COSMO and ROKS/PCM on the ROKS/UKS/PCM optimized geometries opens a way for excited state geometry optimization in solution beyond single-excitation-based theories such as TDA-DFT. As pointed out by us before, the structural differences mainly due to the inclusion of orbital relaxation can be sizable and essential for predictive excited state properties.[55]

Lastly, the comparison of different second-order correlated wavefunction methods emphasizes the favorable accuracy and robustness of ΔDFT/PCM-based methods even for quite distinct properties, which likely require the inclusion of triples to match consistently with correlated wavefunction methods. Hence, UKS/PCM and ROKS/PCM tout themselves as practical methods to compute solvated excited-state geometries, as well as relative and absolute excitation energies of CT states, and as an internal (computationally inexpensive) benchmark for excitation-based methods susceptible to CT errors. Such a mixed protocol combines the practical benefits of excitation-based methods, such as fast access to many low-lying excited states and their transition properties, with accuracy beyond second-order correlated wavefunction methods at a fraction of their cost.

Conflicts of interest

There are no conflicts to declare.

Data availability

Any additional information can be obtained from the corresponding author upon reasonable request.

All data supporting this study are provided in the main article and its SI. The SI contains a compressed archive (.zip) with all output files and structures which allow to reproduce every calculation reported. The molecular geometries employed were taken verbatim from the published STGABS27 and STGABS27-EMS benchmark studies. The SI also contains computational details; CC2 singlet–triplet gaps and emission energies; a comparison of ADC(2) and CC2; basis set effects for the singlet–triplet gaps; solvation effects for singlet–triplet gaps and emission energies; definitions of statistical measures. See DOI: **https://doi.org/10.1039/d5cp02144h**

Acknowledgements

The authors thank Prof. Stefan Grimme for granting access to the computational resources at the Mulliken Center for Theoretical Chemistry. T. F. acknowledges the Fonds der Chemischen Industrie (FCI) for funding under a Kekulé scholarship. C. H. acknowledges financial support by the Deutsche Forschungsgemeinschaft (DFG, German Research Foundation) under Germany's Excellence Strategy EXC 2033-390677874-RESOLV.

References

1 M. Wormit, P. H. P. Harbach, J. M. Mewes, S. Amarie, J. Wachtveitl and A. Dreuw, Excitation energy transfer and carotenoid radical cation formation in light harvesting complexes—A theoretical perspective, *Biochim. Biophys. Acta, Bioenerg.*, 2009, **1787**, 738–746.

2 A. Sirohiwal and D. A. Pantazis, Reaction Center Excitation in Photosystem II: From Multiscale Modeling to Functional Principles, *Acc. Chem. Res.*, 2023, **56**, 2921–2932.

3 A. Forde, S. Maity, V. M. Freixas, S. Fernandez-Alberti, A. J. Neukirch, U. Kleinekathöfer and S. Tretiak, Stabilization of Charge-Transfer Excited States in Biological Systems: A Computational Focus on the Special Pair in Photosystem II Reaction Centers, *J. Phys. Chem. Lett.*, 2024, **15**, 4142–4150.

4 D.-T. Nguyen and T.-O. Do, Comprehensive Review for an Efficient Charge Transfer in Single Atomic Site Catalyst/Organic Polymers toward Photocatalytic CO_2 Reduction, *Adv. Mater. Interfaces*, 2023, **10**, 2201413.

5 M. Akita, P. Ceroni, C. R. J. Stephenson and G. Masson, Progress in Photocatalysis for Organic Chemistry, *J. Org. Chem.*, 2023, **88**, 6281–6283.
6 A. Marie May and J. L. Dempsey, A new era of LMCT: leveraging ligand-to-metal charge transfer excited states for photochemical reactions, *Chem. Sci.*, 2024, **15**, 6661–6678.
7 X.-K. Chen, V. Coropceanu and J.-L. Brédas, Assessing the nature of the charge-transfer electronic states in organic solar cells, *Nat. Commun.*, 2018, **9**, 5295.
8 J. Hustings, R. Bonné, R. Cornelissen, F. Morini, R. Valcke, K. Vandewal and J. V. Manca, Charge-transfer states in photosynthesis and organic solar cells, *Front. Photonics*, 2022, **3**, 1050189.
9 H. Yersin, R. Czerwieniec, L. Mataranga-Popa, J.-M. Mewes, G. Cheng, C.-M. Che, M. Saigo, S. Kimura, K. Miyata and K. Onda, Eliminating the Reverse ISC Bottleneck of TADF Through Excited State Engineering and Environment-Tuning Toward State Resonance Leading to Mono-Exponential Sub-μs Decay. High OLED External Quantum Efficiency Confirms Efficient Exciton Harvesting, *Adv. Funct. Mater.*, 2022, **32**, 2201772.
10 A. L. Schleper, K. Goushi, C. Bannwarth, B. Haehnle, P. J. Welscher, C. Adachi and A. J. C. Kuehne, Hot exciplexes in U-shaped TADF molecules with emission from locally excited states, *Nat. Commun.*, 2021, **12**, 6179.
11 A. L. Schleper, S. Hillebrandt, C. Bannwarth, A. Mischok, S. Kwon, F. Buchner, F. Tenopala-Carmona, R. J. Behm, F. D. Goll, P. J. Welscher, M. Usselmann, U. Ziener, M. C. Gather and A. J. C. Kuehne, Influence of regioisomerism in bis(terpyridine) based exciplexes with delayed fluorescence, *J. Mater. Chem. C*, 2022, **10**, 7699–7706.
12 Z. Xie, C. Cao, Y. Zou, X. Cao, C. Zhou, J. He, C.-S. Lee and C. Yang, Molecular Engineering Enables TADF Emitters Well Suitable for Non-Doped OLEDs with External Quantum Efficiency of Nearly 30%, *Adv. Funct. Mater.*, 2022, **32**, 2112881.
13 A. S. Scholz, J. G. Massoth, L. Stoess, M. Bolte, M. Braun, H.-W. Lerner, J.-M. Mewes, M. Wagner and T. Froitzheim, NBN- and BNB-Phenalenyls: the Yin and Yang of Heteroatom-doped π Systems, *Chem. – Eur. J.*, 2024, **30**, e202400320.
14 A. S. Scholz, T. Froitzheim, M. Bolte, H.-W. Lerner, J.-M. Mewes and M. Wagner, NBN/BNB-doped phenalenyl homo- and heterodyads: structural uniformity but optoelectronic diversity, *Org. Chem. Front.*, 2024, **11**, 3109–3118.
15 M. Barbatti, When theory came first: a review of theoretical chemical predictions ahead of experiments, *Pure Appl. Chem.*, 2025, DOI: **10.1515/pac-2025-0455**.
16 B. Kozma, A. Tajti, B. Demoulin, R. Izsák, M. Nooijen and P. G. Szalay, A New Benchmark Set for Excitation Energy of Charge Transfer States: Systematic Investigation of Coupled Cluster Type Methods, *J. Chem. Theory Comput.*, 2020, **16**, 4213–4225.
17 P.-F. Loos, M. Comin, X. Blase and D. Jacquemin, Reference Energies for Intramolecular Charge-Transfer Excitations, *J. Chem. Theory Comput.*, 2021, **17**, 3666–3686.
18 M. Véril, A. Scemama, M. Caffarel, F. Lipparini, M. Boggio-Pasqua, D. Jacquemin and P.-F. Loos, QUESTDB: a database of highly accurate excitation energies for the electronic structure community, *Wiley Interdiscip. Rev.: Comput. Mol. Sci.*, 2021, **11**, e1517.
19 D. Mester and M. Kállay, Charge-Transfer Excitations within Density Functional Theory: How Accurate Are the Most Recommended Approaches?, *J. Chem. Theory Comput.*, 2022, **18**, 1646–1662.
20 N. Bogo and C. J. Stein, Benchmarking DFT-based excited-state methods for intermolecular charge-transfer excitations, *Phys. Chem. Chem. Phys.*, 2024, **26**, 21575–21588.
21 N. T. Tran and L. N. Tran, Attaining high accuracy for charge-transfer excitations in non-covalent complexes at second-order perturbation cost: the importance of state-specific self-consistency, *J. Chem. Phys.*, 2025, **162**, 104109.
22 Q. Zhang, B. Li, S. Huang, H. Nomura, H. Tanaka and C. Adachi, Efficient blue organic light-emitting diodes employing thermally activated delayed fluorescence, *Nat. Photonics*, 2014, **8**, 326–332.
23 F. B. Dias, T. J. Penfold and A. P. Monkman, Photophysics of thermally activated delayed fluorescence molecules, *Methods Appl. Fluoresc.*, 2017, **5**, 012001.
24 Z. Yang, Z. Mao, Z. Xie, Y. Zhang, S. Liu, J. Zhao, J. Xu, Z. Chi and M. P. Aldred, Recent advances in organic thermally activated delayed fluorescence materials, *Chem. Soc. Rev.*, 2017, **46**, 915–1016.
25 M. Y. Wong and E. Zysman-Colman, Purely Organic Thermally Activated Delayed Fluorescence Materials for Organic Light-Emitting Diodes, *Adv. Mater.*, 2017, **29**, 1605444.
26 T. Huang, W. Jiang and L. Duan, Recent progress in solution processable TADF materials for organic lightemitting diodes, *J. Mater. Chem. C*, 2018, **6**, 5577–5596.
27 J.-M. Mewes, Modeling TADF in organic emitters requires a careful consideration of the environment and going beyond the Franck–Condon approximation, *Phys. Chem. Chem. Phys.*, 2018, **20**, 12454–12469.
28 H. Uoyama, K. Goushi, K. Shizu, H. Nomura and C. Adachi, Highly efficient organic light-emitting diodes from delayed fluorescence, *Nature*, 2012, **492**, 234–238.
29 M. N. Berberan-Santos and J. M. M. Garcia, Unusually Strong Delayed Fluorescence of C70, *J. Am. Chem. Soc.*, 1996, **118**, 9391–9394.
30 L. Kunze, A. Hansen, S. Grimme and J. M. Mewes, PCM-ROKS for the Description of Charge-Transfer States in Solution: Singlet–Triplet Gaps with Chemical Accuracy from Open-Shell Kohn-Sham Reaction-Field Calculations, *J. Phys. Chem. Lett.*, 2021, **12**, 8470–8480.
31 I. Okazaki, F. Sato, T. Yoshihiro, T. Ueno and H. Kashiwagi, Development of a restricted open shell Kohn–Sham program and its application to a model heme complex, *THEOCHEM*, 1998, **451**, 109–119.
32 I. Frank, J. Hutter, D. Marx and M. Parrinello, Molecular dynamics in low-spin excited states, *J. Chem. Phys.*, 1998, **108**, 4060–4069.
33 M. Filatov and S. Shaik, Application of spin-restricted open-shell Kohn–Sham method to atomic and molecular multiplet states, *J. Chem. Phys.*, 1999, **110**, 116–125.

34 S. R. Billeter and D. Egli, Calculation of nonadiabatic couplings with restricted open-shell Kohn-Sham density functional theory, *J. Chem. Phys.*, 2006, **125**, 224103.
35 M. Schulte and I. Frank, Restricted open-shell Kohn–Sham theory: N unpaired electrons, *Chem. Phys.*, 2010, **373**, 283–288.
36 T. Kowalczyk, T. Tsuchimochi, P.-T. Chen, L. Top and T. Van Voorhis, Excitation energies and Stokes shifts from a restricted open-shell Kohn-Sham approach, *J. Chem. Phys.*, 2013, **138**, 164101.
37 A. T. B. Gilbert, N. A. Besley and P. M. W. Gill, Self-Consistent Field Calculations of Excited States Using the Maximum Overlap Method (MOM), *J. Phys. Chem. A*, 2008, **112**, 13164–13171.
38 G. M. J. Barca, A. T. B. Gilbert and P. M. W. Gill, Excitation Number: Characterizing Multiply Excited States, *J. Chem. Theory Comput.*, 2018, **14**, 9–13.
39 S. Miertuš, E. Scrocco and J. Tomasi, Electrostatic interaction of a solute with a continuum. A direct utilization of AB initio molecular potentials for the prevision of solvent effects, *Chem. Phys.*, 1981, **55**, 117–129.
40 J. M. Herbert, Dielectric continuum methods for quantum chemistry, *Wiley Interdiscip. Rev.: Comput. Mol. Sci.*, 2021, **11**, e1519.
41 T. Stein, L. Kronik and R. Baer, Reliable Prediction of Charge Transfer Excitations in Molecular Complexes Using Time-Dependent Density Functional Theory, *J. Am. Chem. Soc.*, 2009, **131**, 2818–2820.
42 T. Stein, L. Kronik and R. Baer, Prediction of charge-transfer excitations in coumarin-based dyes using a range-separated functional tuned from first principles, *J. Chem. Phys.*, 2009, **131**, 244119.
43 T. Stein, H. Eisenberg, L. Kronik and R. Baer, Fundamental Gaps in Finite Systems from Eigenvalues of a Generalized Kohn-Sham Method, *Phys. Rev. Lett.*, 2010, **105**, 266802.
44 R. Baer, E. Livshits and U. Salzner, Tuned Range-Separated Hybrids in Density Functional Theory, *Annu. Rev. Phys. Chem.*, 2010, **61**, 85–109.
45 L. Kronik, T. Stein, S. Refaely-Abramson and R. Baer, Excitation Gaps of Finite-Sized Systems from Optimally Tuned Range-Separated Hybrid Functionals, *J. Chem. Theory Comput.*, 2012, **8**, 1515–1531.
46 N. Mardirossian and M. Head-Gordon, ωB97M-V: a combinatorially optimized, range-separated hybrid, meta-GGA density functional with VV10 nonlocal correlation, *J. Chem. Phys.*, 2016, **144**, 214110.
47 O. A. Vydrov and T. Van Voorhis, Nonlocal van der Waals density functional: the simpler the better, *J. Chem. Phys.*, 2010, **133**, 244103.
48 T. Froitzheim, L. Kunze, S. Grimme, J. M. Herbert and J.-M. Mewes, Benchmarking Charge-Transfer Excited States in TADF Emitters: ΔDFT Outperforms TD-DFT for Emission Energies, *J. Phys. Chem. A*, 2024, **128**, 6324–6335.
49 C. Adamo and V. Barone, Toward reliable density functional methods without adjustable parameters: the PBE0 model, *J. Chem. Phys.*, 1999, **110**, 6158.
50 E. Caldeweyher, C. Bannwarth and S. Grimme, Extension of the D3 dispersion coefficient model, *J. Chem. Phys.*, 2017, **147**, 034112.
51 E. Caldeweyher, J.-M. Mewes, S. Ehlert and S. Grimme, Extension and evaluation of the D4 London-dispersion model for periodic systems, *Phys. Chem. Chem. Phys.*, 2020, **22**, 8499–8512.
52 M. A. Rohrdanz and J. M. Herbert, Simultaneous benchmarking of ground- and excited-state properties with long-range-corrected density functional theory, *J. Chem. Phys.*, 2008, **129**, 034107.
53 E. Runge and E. K. U. Gross, Density-Functional Theory for Time-Dependent Systems, *Phys. Rev. Lett.*, 1984, **52**, 997–1000.
54 S. Hirata and M. Head-Gordon, Time-dependent density functional theory within the Tamm–Dancoff approximation, *Chem. Phys. Lett.*, 1999, **314**, 291–299.
55 T. Froitzheim, S. Grimme and J.-M. Mewes, Either Accurate Singlet–Triplet Gaps or Excited-State Structures: Testing and Understanding the Performance of TD-DFT for TADF Emitters, *J. Chem. Theory Comput.*, 2022, **18**, 7702–7713.
56 R. Khatri and B. D. Dunietz, Accurate Singlet–Triplet Excited States Energy Gap Can Be Mastered by Time-Dependent Density Functional Theory Calculations Based on a Dielectric-Screened Range-Separated Hybrid Functional, *J. Phys. Chem. C*, 2024, **129**(1), 436–446.
57 T. Hatakeyama, K. Shiren, K. Nakajima, S. Nomura, S. Nakatsuka, K. Kinoshita, J. Ni, Y. Ono and T. Ikuta, Ultrapure Blue Thermally Activated Delayed Fluorescence Molecules: Efficient HOMO–LUMO Separation by the Multiple Resonance Effect, *Adv. Mater.*, 2016, **28**, 2777–2781.
58 P. de Silva, Inverted Singlet–Triplet Gaps and Their Relevance to Thermally Activated Delayed Fluorescence, *J. Phys. Chem. Lett.*, 2019, **10**, 5674–5679.
59 N. Aizawa, Y.-J. Pu, Y. Harabuchi, A. Nihonyanagi, R. Ibuka, H. Inuzuka, B. Dhara, Y. Koyama, K.-I. Nakayama, S. Maeda, F. Araoka and D. Miyajima, Delayed fluorescence from inverted singlet and triplet excited states, *Nature*, 2022, **609**, 502–506.
60 L. Wrigley and C. W. Schlenker, Singlet-Triplet Inversion, *Annu. Rev. Phys. Chem.*, 2025, **76**, 329–355.
61 L. Kunze, T. Froitzheim, A. Hansen, S. Grimme and J.-M. Mewes, ΔDFT Predicts Inverted Singlet–Triplet Gaps with Chemical Accuracy at a Fraction of the Cost of Wave Function-Based Approaches, *J. Phys. Chem. Lett.*, 2024, 8065–8077.
62 L. Kunze, A. Hansen, S. Grimme and J.-M. Mewes, The Best of Both Worlds: ΔDFT Describes Multiresonance TADF Emitters with Wave-Function Accuracy at Density-Functional Cost, *J. Phys. Chem. Lett.*, 2025, **16**, 1114–1125.
63 A. Dreuw and M. Head-Gordon, Failure of Time-Dependent Density Functional Theory for Long-Range Charge-Transfer Excited States: The Zincbacteriochlorin-Bacteriochlorin and Bacteriochlorophyll-Spheroidene Complexes, *J. Am. Chem. Soc.*, 2004, **126**, 4007–4016.

64 A. Dreuw and M. Head-Gordon, Single-Reference ab Initio Methods for the Calculation of Excited States of Large Molecules, *Chem. Rev.*, 2005, **105**, 4009–4037.
65 J. Neugebauer, O. Gritsenko and E. J. Baerends, Assessment of a simple correction for the long-range charge-transfer problem in time-dependent density-functional theory, *J. Chem. Phys.*, 2006, **124**, 214102.
66 J. E. Subotnik, Communication: configuration interaction singles has a large systematic bias against chargetransfer states, *J. Chem. Phys.*, 2011, **135**, 071104.
67 S. Grimme and M. Waletzke, A combination of Kohn–Sham density functional theory and multireference configuration interaction methods, *J. Chem. Phys.*, 1999, **111**, 5645–5655.
68 C. M. Marian, A. Heil and M. Kleinschmidt, The DFT/MRCI method, *Wiley Interdiscip. Rev.: Comput. Mol. Sci.*, 2019, **9**, e1394.
69 M. Pauls, T. Froitzheim, A. Torgashov, J.-M. Mewes, S. Grimme and C. Bannwarth, On the Performance of DFT/MRCI for Singlet–Triplet Gaps and Emission Energies of Thermally Activated Delayed Fluorescence Molecules, *ChemRxiv*, 2025, DOI: **10.26434/chemrxiv-2025-8910n**.
70 O. Christiansen, H. Koch and P. Jørgensen, The secondorder approximate coupled cluster singles and doubles model CC2, *Chem. Phys. Lett.*, 1995, **243**, 409–418.
71 K. Sneskov and O. Christiansen, Excited state coupled cluster methods, *Wiley Interdiscip. Rev.: Comput. Mol. Sci.*, 2012, **2**, 566–584.
72 R. Izsák, Single-reference coupled cluster methods for computing excitation energies in large molecules: the efficiency and accuracy of approximations, *Wiley Interdiscip. Rev.: Comput. Mol. Sci.*, 2020, **10**, e1445.
73 J. Schirmer, Beyond the random-phase approximation: a new approximation scheme for the polarization propagator, *Phys. Rev. A: At., Mol., Opt. Phys.*, 1982, **26**, 2395–2416.
74 A. B. Trofimov and J. Schirmer, An efficient polarization propagator approach to valence electron excitation spectra, *J. Phys. B: At., Mol. Opt. Phys.*, 1995, **28**, 2299.
75 M. Wormit, D. R. Rehn, P. H. Harbach, J. Wenzel, C. M. Krauter, E. Epifanovsky and A. Dreuw, Investigating excited electronic states using the algebraic diagrammatic construction (ADC) approach of the polarization propagator, *Mol. Phys.*, 2014, **112**, 774–784.
76 A. Dreuw and M. Wormit, The algebraic diagrammatic construction scheme for the polarization propagator for the calculation of excited states, *Wiley Interdiscip. Rev.: Comput. Mol. Sci.*, 2015, **5**, 82–95.
77 H. Koch, H. J. A. Jensen, P. Jørgensen and T. Helgaker, Excitation energies from the coupled cluster singles and doubles linear response function (CCSDLR). Applications to Be, CH^+, CO, and H_2O, *J. Chem. Phys.*, 1990, **93**, 3345–3350.
78 C. Hättig, Response Theory and Molecular Properties (A Tribute to Jan Linderberg and Poul Jørgensen), in *Advances in Quantum Chemistry*, ed. H. J. A. Jensen, Academic Press, 2005, vol. 50, pp. 37–60.
79 C. Hättig and F. Weigend, CC2 excitation energy calculations on large molecules using the resolution of the identity approximation, *J. Chem. Phys.*, 2000, **113**, 5154–5161.
80 A. Hellweg, S. A. Grün and C. Hättig, Benchmarking the performance of spin-component scaled CC2 in ground and electronically excited states, *Phys. Chem. Chem. Phys.*, 2008, **10**, 4119–4127.
81 S. Grimme, Improved second-order Møller–Plesset perturbation theory by separate scaling of parallel- and antiparallel-spin pair correlation energies, *J. Chem. Phys.*, 2003, **118**, 9095–9102.
82 A. Szabados, Theoretical interpretation of Grimme's spin-component-scaled second order Møller-Plesset theory, *J. Chem. Phys.*, 2006, **125**, 214105.
83 S. Grimme, L. Goerigk and R. F. Fink, Spin-component-scaled electron correlation methods, *Wiley Interdiscip. Rev.: Comput. Mol. Sci.*, 2012, **2**, 886–906.
84 A. Tajti, J. F. Stanton, D. A. Matthews and P. G. Szalay, Accuracy of Coupled Cluster Excited State Potential Energy Surfaces, *J. Chem. Theory Comput.*, 2018, **14**, 5859–5869.
85 A. Tajti and P. G. Szalay, Accuracy of Spin-Component-Scaled CC2 Excitation Energies and Potential Energy Surfaces, *J. Chem. Theory Comput.*, 2019, **15**, 5523–5531.
86 A. Tajti, L. Tulipán and P. G. Szalay, Accuracy of Spin-Component Scaled ADC(2) Excitation Energies and Potential Energy Surfaces, *J. Chem. Theory Comput.*, 2020, **16**, 468–474.
87 Y. Jung, R. C. Lochan, A. D. Dutoi and M. Head-Gordon, Scaled opposite-spin second order Møller–Plesset correlation energy: an economical electronic structure method, *J. Chem. Phys.*, 2004, **121**, 9793–9802.
88 N. O. C. Winter and C. Hättig, Scaled opposite-spin CC2 for ground and excited states with fourth order scaling computational costs, *J. Chem. Phys.*, 2011, **134**, 184101.
89 B. Helmich and C. Hättig, A pair natural orbital implementation of the coupled cluster model CC2 for excitation energies, *J. Chem. Phys.*, 2013, **139**, 084114.
90 C. Neiss, C. Hättig and W. Klopper, Extensions of r12 corrections to CC2-R12 for excited states, *J. Chem. Phys.*, 2006, **125**, 064111.
91 C. Hättig, in *Computational Nanoscience: Do It Yourself!*, ed. J. Grotendorst, S. Blügel and D. Marx, NIC series 31; NIC-Secretariat, Research Centre Jülich, Jülich, 2006, pp. 245–278.
92 M. Schreiber, M. R. Silva-Junior, S. P. A. Sauer and W. Thiel, Benchmarks for electronically excited states: CASPT2, CC2, CCSD, and CC3, *J. Chem. Phys.*, 2008, **128**, 134110.
93 P.-F. Loos, A. Scemama, A. Blondel, Y. Garniron, M. Caffarel and D. Jacquemin, A Mountaineering Strategy to Excited States: Highly Accurate Reference Energies and Benchmarks, *J. Chem. Theory Comput.*, 2018, **14**, 4360–4379.
94 P.-F. Loos, F. Lipparini, M. Boggio-Pasqua, A. Scemama and D. Jacquemin, A Mountaineering Strategy to Excited States: Highly Accurate Energies and Benchmarks for Medium Sized Molecules, *J. Chem. Theory Comput.*, 2020, **16**, 1711–1741.

95 D. Jacquemin, I. Duchemin and X. Blase, 0–0 Energies Using Hybrid Schemes: Benchmarks of TD-DFT, CIS(D), ADC(2), CC2, and BSE/GW formalisms for 80 Real-Life Compounds, *J. Chem. Theory Comput.*, 2015, **11**, 5340–5359.
96 N. O. C. Winter, N. K. Graf, S. Leutwyler and C. Hättig, Benchmarks for 0–0 transitions of aromatic organic molecules: DFT/B3LYP, ADC(2), CC2, SOS-CC2 and SCS-CC2 compared to high-resolution gas-phase data, *Phys. Chem. Chem. Phys.*, 2013, **15**, 6623–6630.
97 D. Kánnár and P. G. Szalay, Benchmarking Coupled Cluster Methods on Valence Singlet Excited States, *J. Chem. Theory Comput.*, 2014, **10**, 3757–3765.
98 R. Sarkar, M. Boggio-Pasqua, P.-F. Loos and D. Jacquemin, Benchmarking TD-DFT and Wave Function Methods for Oscillator Strengths and Excited-State Dipole Moments, *J. Chem. Theory Comput.*, 2021, **17**, 1117–1132.
99 J. F. Stanton and R. J. Bartlett, The equation of motion coupled-cluster method. A systematic biorthogonal approach to molecular excitation energies, transition probabilities, and excited state properties, *J. Chem. Phys.*, 1993, **98**, 7029–7039.
100 A. I. Krylov, Equation-of-Motion Coupled-Cluster Methods for Open-Shell and Electronically Excited Species: The Hitchhiker's Guide to Fock Space, *Annu. Rev. Phys. Chem.*, 2008, **59**, 433–462.
101 R. J. Bartlett, Coupled-cluster theory and its equation-of-motion extensions, *Wiley Interdiscip. Rev.: Comput. Mol. Sci.*, 2012, **2**, 126–138.
102 P. H. P. Harbach, M. Wormit and A. Dreuw, The thirdorder algebraic diagrammatic construction method (ADC(3)) for the polarization propagator for closed-shell molecules: efficient implementation and benchmarking, *J. Chem. Phys.*, 2014, **141**, 064113.
103 A. Tajti and P. G. Szalay, Investigation of the Impact of Different Terms in the Second Order Hamiltonian on Excitation Energies of Valence and Rydberg States, *J. Chem. Theory Comput.*, 2016, **12**, 5477–5482.
104 T. J. J. Watson, V. F. Lotrich, P. G. Szalay, A. Perera and R. J. Bartlett, Benchmarking for Perturbative Triple-Excitations in EE-EOM-CC Methods, *J. Phys. Chem. A*, 2013, **117**, 2569–2579.
105 P.-F. Loos and D. Jacquemin, Is ADC(3) as Accurate as CC3 for Valence and Rydberg Transition Energies?, *J. Phys. Chem. Lett.*, 2020, **11**, 974–980.
106 H. Koch, O. Christiansen, P. Jørgensen, A. M. Sanchez de Merás and T. Helgaker, The CC3 model: an iterative coupled cluster approach including connected triples, *J. Chem. Phys.*, 1997, **106**, 1808–1818.
107 R. Cammi, S. Corni, B. Mennucci and J. Tomasi, Electronic excitation energies of molecules in solution: state specific and linear response methods for nonequilibrium continuum solvation models, *J. Chem. Phys.*, 2005, **122**, 104513.
108 M. Caricato, A comparison between state-specific and linear-response formalisms for the calculation of vertical electronic transition energy in solution with the CCSD-PCM method, *J. Chem. Phys.*, 2013, **139**, 044116.
109 J. M. Mewes, Z. Q. You, M. Wormit, T. Kriesche, J. M. Herbert and A. Dreuw, Experimental benchmark data and systematic evaluation of two a posteriori, polarizable-continuum corrections for vertical excitation energies in solution, *J. Phys. Chem. A*, 2015, **119**, 5446–5464.
110 J. M. Mewes, J. M. Herbert and A. Dreuw, On the accuracy of the general, state-specific polarizable-continuum model for the description of correlated ground- and excited states in solution, *Phys. Chem. Chem. Phys.*, 2017, **19**, 1644–1654.
111 S. K. Khani, A. M. Khah and C. Hättig, COSMO-RI-ADC(2) excitation energies and excited state gradients, *Phys. Chem. Chem. Phys.*, 2018, **20**, 16354–16363.
112 M. Caricato, B. Mennucci, J. Tomasi, F. Ingrosso, R. Cammi, S. Corni and G. Scalmani, Formation and relaxation of excited states in solution: a new time dependent polarizable continuum model based on time dependent density functional theory, *J. Chem. Phys.*, 2006, **124**, 124520.
113 R. Improta, G. Scalmani, M. J. Frisch and V. Barone, Toward effective and reliable fluorescence energies in solution by a new state specific polarizable continuum model time dependent density functional theory approach, *J. Chem. Phys.*, 2007, **127**, 074504.
114 C. A. Guido, A. Chrayteh, G. Scalmani, B. Mennucci and D. Jacquemin, Simple Protocol for Capturing Both Linear-Response and State-Specific Effects in Excited-State Calculations with Continuum Solvation Models, *J. Chem. Theory Comput.*, 2021, **17**, 5155–5164.
115 M. Caricato, Absorption and Emission Spectra of Solvated Molecules with the EOM–CCSD–PCM Method, *J. Chem. Theory Comput.*, 2012, **8**, 4494–4502.
116 M. Caricato, Exploring Potential Energy Surfaces ofv Electronic Excited States in Solution with the EOM-CCSD-PCM Method, *J. Chem. Theory Comput.*, 2012, **8**, 5081–5091.
117 C. Hättig and A. Pausch, Gradients of Ground and Excited States for CC2 and ADC(2) in Polarizable Continuum and Atomistic Embeddings within a Generalized PTED Coupling Scheme, *J. Phys. Chem. A*, 2025, **129**, 6155–6169.
118 J. Franck and E. G. Dymond, Elementary processes of photochemical reactions, *Trans. Faraday Soc.*, 1926, **21**, 536–542.
119 E. Condon, A Theory of Intensity Distribution in Band Systems, *Phys. Rev.*, 1926, **28**, 1182–1201.
120 S. Grimme, J. G. Brandenburg, C. Bannwarth and A. Hansen, Consistent structures and interactions by density functional theory with small atomic orbital basis sets, *J. Chem. Phys.*, 2015, **143**, 054107.
121 C. Hättig and A. Köhn, Transition moments and excited-state first-order properties in the coupled-cluster model CC2 using the resolution-of-the-identity approximation, *J. Chem. Phys.*, 2002, **117**, 6939–6951.
122 C. Hättig, A. Köhn and K. Hald, First-order properties for triplet excited states in the approximated coupled cluster model CC2 using an explicitly spin coupled basis, *J. Chem. Phys.*, 2002, **116**, 5401–5410.
123 C. Hättig and K. Hald, Implementation of RI-CC2 triplet excitation energies with an application to trans-azobenzene, *Phys. Chem. Chem. Phys.*, 2002, **4**, 2111–2118.

124 C. Hättig, A. Hellweg and A. Köhn, Distributed memory parallel implementation of energies and gradients for second-order Møller–Plesset perturbation theory with the resolution-of-the-identity approximation, *Phys. Chem. Chem. Phys.*, 2006, **8**, 1159–1169.
125 TURBOMOLE V7.7 2022, a development of University of Karlsruhe and Forschungszentrum Karlsruhe GmbH, 1989–2007, TURBOMOLE GmbH, since 2007, available from **https://www.turbomole.org**.
126 S. G. Balasubramani, *et al.*, TURBOMOLE: modular program suite for ab initio quantum-chemical and condensed-matter simulations, *J. Chem. Phys.*, 2020, **152**, 184107.
127 Y. J. Franzke, *et al.*, TURBOMOLE: Today and Tomorrow, *J. Chem. Theory Comput.*, 2023, **19**, 6859–6890.
128 B. Lunkenheimer and A. Köhn, Solvent Effects on Electronically Excited States Using the Conductor-Like Screening Model and the Second-Order Correlated Method ADC(2), *J. Chem. Theory Comput.*, 2013, **9**, 977–994.
129 A. Klamt and G. Schüürmann, COSMO: a new approach to dielectric screening in solvents with explicit expressions for the screening energy and its gradient, *J. Chem. Soc., Perkin Trans. 2*, 1993, 799–805.
130 J. Tomasi, B. Mennucci and R. Cammi, Quantum mechanical continuum solvation models, *Chem. Rev.*, 2005, **105**, 2999–3093.
131 B. Mennucci, Polarizable continuum model, *Wiley Interdiscip. Rev.: Comput. Mol. Sci.*, 2012, **2**, 386–404.
132 C. A. Guido and S. Caprasecca, On the description of the environment polarization response to electronic transitions, *Int. J. Quantum Chem.*, 2019, **119**, e25711.
133 A. Pausch, Consistent Analytical Second Derivatives of the Kohn–Sham DFT Energy in the Framework of the Conductor-Like Screening Model through Gaussian Charge Distributions, *J. Chem. Theory Comput.*, 2024, **20**, 3169–3183.
134 S. Yomosa, Theory of the Excited State of Molecular Complex in Solution, *J. Phys. Soc. Jpn.*, 1974, **36**, 1655–1660.
135 R. Bonaccorsi, R. Cimiraglia and J. Tomasi, Ab initio evaluation of absorption and emission transitions for molecular solutes, including separate consideration of orientational and inductive solvent effects, *J. Comput. Chem.*, 1983, **4**, 567–577.
136 S. Corni, R. Cammi, B. Mennucci and J. Tomasi, Electronic excitation energies of molecules in solution within continuum solvation models: investigating the discrepancy between state-specific and linear-response methods, *J. Chem. Phys.*, 2005, **123**, 134512.
137 R. Improta, V. Barone, G. Scalmani and M. J. Frisch, A state-specific polarizable continuum model time dependent density functional theory method for excited state calculations in solution, *J. Chem. Phys.*, 2006, **125**, 054103.
138 R. Cammi, R. Fukuda, M. Ehara and H. Nakatsuji, Symmetry-adapted cluster and symmetry-adapted cluster-configuration interaction method in the polarizable continuum model: theory of the solvent effect on the electronic excitation of molecules in solution, *J. Chem. Phys.*, 2010, **133**, 024104.
139 R. Fukuda, M. Ehara, H. Nakatsuji and R. Cammi, Nonequilibrium solvation for vertical photoemission and photoabsorption processes using the symmetry-adapted cluster–configuration interaction method in the polarizable continuum model, *J. Chem. Phys.*, 2011, **134**, 104109.
140 C. A. Guido, D. Jacquemin, C. Adamo and B. Mennucci, Electronic Excitations in Solution: The Interplay between State Specific Approaches and a Time-Dependent Density Functional Theory Description, *J. Chem. Theory Comput.*, 2015, **11**, 5782–5790.
141 R. Cammi, Coupled-cluster theories for the polarizable continuum model. II. Analytical gradients for excited states of molecular solutes by the equation of motion coupled-cluster method, *Int. J. Quantum Chem.*, 2010, **110**, 3040–3052.
142 S. Chibani, S. Budzák, M. Medved, B. Mennucci and D. Jacquemin, Full cLR-PCM calculations of the solvatochromic effects on emission energies, *Phys. Chem. Chem. Phys.*, 2014, **16**, 26024–26029.
143 R. Cammi and B. Mennucci, Linear response theory for the polarizable continuum model, *J. Chem. Phys.*, 1999, **110**, 9877.
144 O. Christiansen and K. V. Mikkelsen, Coupled cluster response theory for solvated molecules in equilibrium and nonequilibrium solvation, *J. Chem. Phys.*, 1999, **110**, 8348–8360.
145 S. Karbalaei Khani, A. Marefat Khah and C. Hättig, Comparison of Reaction Field Schemes for Coupling Continuum Solvation Models with Wave Function Methods for Excitation Energies, *J. Chem. Theory Comput.*, 2020, **16**, 4554–4564.
146 E. G. McRae, Theory of Solvent Effects on Molecular Electronic Spectra. Frequency Shifts, *J. Phys. Chem.*, 1957, **61**, 562–572.
147 E. Lippert, Spektroskopische Bestimmung des Dipolmomentes aromatischer Verbindungen im ersten angeregten Singulettzustand. Zeitschrift für Elektrochemie, *Ber. Bauforsch.*, 1957, **61**, 962–975.
148 J. E. Brady and P. W. Carr, An analysis of dielectric models of solvatochromism, *J. Phys. Chem.*, 1985, **89**, 5759–5766.
149 A. Klamt, Calculation of UV/Vis Spectra in Solution, *J. Phys. Chem.*, 1996, **100**, 3349–3353.
150 F. Weigend, M. Häser, H. Patzelt and R. Ahlrichs, RIMP2: optimized auxiliary basis sets and demonstration of efficiency, *Chem. Phys. Lett.*, 1998, **294**, 143–152.
151 F. Weigend and R. Ahlrichs, Balanced basis sets of split valence, triple zeta valence and quadruple zeta valence quality for H to Rn: design and assessment of accuracy, *Phys. Chem. Chem. Phys.*, 2005, **7**, 3297–3305.
152 F. Weigend, Accurate Coulomb-fitting basis sets for H to Rn, *Phys. Chem. Chem. Phys.*, 2006, **8**, 1057–1065.
153 D. Drwal, M. Matousek, P. Golub, A. Tucholska, M. Hapka, J. Brabec, L. Veis and K. Pernal, Role of Spin Polarization and Dynamic Correlation in Singlet–Triplet Gap Inversion of Heptazine Derivatives, *J. Chem. Theory Comput.*, 2023, **19**(21), 7606–7616.
154 J. M. Kaminski, T. Böhmer and C. M. Marian, Balancing TADF Properties in π-Bridged Donor–Acceptor Systems by Sterical Constraints: The Best of ThreeWorlds, *J. Phys. Chem. C*, 2024, **128**(33), 13711–13721.

155 J.-M. Mewes, *Development and Application of Methods for the Description of Photochemical Processes in Condensed Phase*, Dissertation, Heidelberg, Heidelberg, 2015.
156 M. A. Rohrdanz, K. M. Martins and J. M. Herbert, A long-range-corrected density functional that performs well for both ground-state properties and timedependent density functional theory excitation energies, including charge-transfer excited states, *J. Chem. Phys.*, 2009, **130**, 054112.
157 D. Jacquemin, V. Wathelet, E. A. Perpète and C. Adamo, Extensive TD-DFT Benchmark: Singlet-Excited States of Organic Molecules, *J. Chem. Theory Comput.*, 2009, **5**, 2420–2435.
158 C. Adamo and D. Jacquemin, The calculations of excited-state properties with Time-Dependent Density Functional Theory, *Chem. Soc. Rev.*, 2013, **42**, 845–856.
159 A. D. Laurent and D. Jacquemin, TD-DFT benchmarks: a review, *Int. J. Quantum Chem.*, 2013, **113**, 2019–2039.
160 F. Sacchetta, F. H. Bangerter, H. Laqua and C. Ochsenfeld, Efficient Low-Scaling Calculation of THC-SOS-LR-CC2 and THC-SOS-ADC(2) Excitation Energies Through Density-Based Integral-Direct Tensor Hypercontraction, *J. Chem. Theory Comput.*, 2025, **21**(10), 5083–5102.
161 N. Sülzner and C. Hättig, Role of Singles Amplitudes in ADC(2) and CC2 for Low-Lying Electronically Excited States, *J. Chem. Theory Comput.*, 2024, **20**, 2462–2474.
162 J.-M. Mewes, V. Jovanović, C. M. Marian and A. Dreuw, On the molecular mechanism of non-radiative decay of nitrobenzene and the unforeseen challenges this simple molecule holds for electronic structure theory, *Phys. Chem. Chem. Phys.*, 2014, **16**, 12393–12406.

